Modern silicon dynamics of a small high-latitude subarctic lake

Petra Zahajská[1,5], Carolina Olid[2], Johanna Stadmark[1], Sherilyn C. Fritz[3], Sophie Opfergelt[4], and Daniel J. Conley[1]

[1]Department of Geology, Lund University, Lund, Sweden
[2]Department of Ecology and Environmental Science, Umeå University, Umeå, Sweden
[3]Department of Earth and Atmospheric Sciences and School of Biological Sciences, University of Nebraska–Lincoln, Lincoln, Nebraska, USA
[4]Earth and Life Institute, Université catholique de Louvain, Louvain-la-Neuve, Belgium
[5]Institute of Geology and Palaeontology, Faculty of Science, Charles University, Prague, Czech Republic

Correspondence: Petra Zahajská (petra.zahajska@geol.lu.se)

Abstract. High biogenic silica (BSi) concentrations occur sporadically in lake sediments throughout the world, however, the processes leading to high BSi concentrations vary. We explored the factors responsible for the high BSi concentration in sediments of a small, high-latitude subarctic lake (Lake 850). The Si budget of this lake had not been fully characterized before to establish the drivers of BSi accumulation in this environment. To do this, we combined measurements of variations in stream discharge, dissolved silica (DSi) concentrations and stable Si isotopes in both lake and stream water with measurements of BSi content in lake sediments. Water, radon, and Si mass balances revealed the importance of groundwater discharge as a main source of DSi to the lake, with groundwater-derived DSi inputs 3 times higher than those from ephemeral stream inlets. After including all external DSi sources (i.e., inlets and groundwater discharge) and estimating the total BSi accumulation in the sediment, we show that diatom production consumes up to 79% of total DSi input. Additionally, low sediment accumulation rates were observed based on the dated gravity core. Our findings thus demonstrate that groundwater discharge and low mass accumulation rate can account for the high BSi accumulation during the last 150 cal. yr BP. Globally, lakes have been estimated to retain one fifth of the annual DSi terrestrial weathering flux that would otherwise be delivered to the ocean. Well constrained lake mass balances, such as presented here, bring clarity to those estimates of the terrestrial Si cycle sinks.

1 Introduction

Diatoms – unicellular golden-brown algae – are found worldwide in all aquatic environments, wetlands, and soils (Battarbee et al., 2002; Clarke, 2003). Diatoms take up dissolved silicic acid, H_4SiO_4, expressed here as dissolved silica (DSi), and build their shells in the form of amorphous silica, also known as biogenic silica (BSi). Diatom production is thus a crucial component in the global Si cycle (Tréguer and De La Rocha, 2013). Massive accumulations of fossil diatom frustules in sediments have been observed in multiple lakes situated in silicon-rich environments, especially on volcanic bedrock, such as Lake Challa, Tanzania/Kenya (Barker et al., 2013), or in hydrothermally active areas, such as Yellowstone Lake, US (Theriot et al., 2006) or Lake Myvatn, Iceland (Opfergelt et al., 2011). However, lakes without volcanism can also accumulate high concentrations of BSi in the sediment (Frings et al., 2014). One example is high-elevation and high-latitude lakes, where BSi concentrations as

high as 60 weight percent of SiO_2 have been found (Frings et al., 2014; Rosén et al., 2010). In addition, high BSi concentrations in sediment have been observed in Lough Neagh, Northern Ireland (Plunkett et al., 2004), Lake Baikal (Swann and Mackay, 2006), Lake Edward (Russell and Johnson, 2005), and Lake Malawi (Johnson et al., 2011). The processes responsible for the diatom-rich sediment formation in these non-volcanic settings, however, are poorly understood.

High BSi accumulation in sediment has been hypothesized to require sufficient DSi in the water column for diatoms to grow and low detrital input to minimize dilution of autochthonous BSi (Conger, 1942). DSi originates ultimately from weathering of bedrock, and it is transported by rivers through the environment where it can be removed by biological or chemical processes, such as secondary clay mineral formation or amorphous silica precipitation (Jenny, 1941). DSi concentrations in the environment are influenced by factors, such as vegetation type (Jenny, 1941; Leng et al., 2009; Struyf et al., 2010), bedrock type (Jenny, 1941; Opfergelt and Delmelle, 2012), indirectly by climate forcing (Fortin and Gajewski, 2009; Jenny, 1941), or watershed geomorphology (Jenny, 1941). In particular, attention has been paid to the relative importance of groundwater discharge as a main source of DSi for a few lakes, such as Lake O'Hara, British Columbia (Hood et al., 2006), Lake Myvatn, Iceland (Opfergelt et al., 2011), Crystal Lake, Wisconsin (Kenoyer and Anderson, 1989; Hurley et al., 1985), at the mouth of the Changjiang river system, China (Zhang et al., 2020), and in Canadian and Siberian rivers (Maavara et al., 2018; Pokrovsky et al., 2013). However, the significance of groundwater discharge is still often overlooked in studies about Si dynamics in lakes.

The contribution of groundwater to lake Si cycle can be evaluated using Si isotopes. Stable Si isotopes are used to trace variation in DSi sources or diatom production and discern processes affecting BSi accumulation in lake sediments. Among the three stable isotopes (^{28}Si, ^{29}Si and ^{29}Si) diatoms preferentially take up the lighter ^{28}Si (De La Rocha et al., 1997). Diatoms tend to fractionate the Si isotopes with a fractionation factor of -1.1 ‰ (De La Rocha et al., 1997), which means that the diatom BSi will have an isotopically lighter ratio compared to the source DSi. Riverine DSi usually shows isotopically heavier ratios compared to groundwater, as there are more processes that fractionate Si isotopes during river transport (Frings et al., 2016; Opfergelt and Delmelle, 2012; Sutton et al., 2018). Therefore, stable Si isotopes are an ideal tracer for the contribution of groundwater.

Here, we investigate the diatom-rich sediment formation in Lake 850 through water and silicon mass balances. Lake 850, northernmost Sweden, is an ideal case study with a high content of BSi in the sediment ca. 40 weight percent (wt%) (Rosén et al., 2010). Oxygen isotopes from diatoms suggested that the lake's isotopic ratio is mostly influenced by summer precipitation and variations in the ephemeral inlet streams (Shemesh et al., 2001). Unlike previous studies in this lake, we hypothesize that groundwater discharge is an important mechanism controlling lake DSi concentrations. To test this hypothesis, we estimate groundwater flows discharging into the lake using a water and a radon (^{222}Rn) mass balance. DSi concentration and stable Si isotope mass balances were used to determine Si sources for the diatom-rich sediment deposited during recent decades.

2 Study area

Lake 850 (68°15′ N, 19°7′ E) is located $14\,km$ southeast from the Abisko Research Station (388 m a.s.l.), northern Sweden. From 1913 to 2019, the mean annual surface atmospheric temperature was $-0.4\,°C$, whereas during the study years (2018-

2019) the mean annual temperature was $0.03\,°\text{C}$. Further, the mean surface atmospheric temperature during the aquatic growing season in 2018-2019 (June to August) was $10.1\,°\text{C}$ (1SD = $2.8\,°\text{C}$), and the long-term (1913-2019) mean summer temperature of $9.8\,°\text{C}$ (1SD = $3.6\,°\text{C}$) (ANS, 2020a). During the ice-free period direct surface precipitation contribution from the watershed was estimated from the mean precipitation of $48\,\text{mm}\,\text{month}^{-1}$ (ANS, 2020a). Lake 850 lies above the tree-limit (600 m a.s.l) at 850 m a.s.l. The lake surface area is $0.02\,\text{km}^2$, with a maximum depth of $8\,\text{m}$ and a catchment area of $0.35\,\text{km}^2$ (Rubensdotter and Rosqvist, 2003). Lake deep basin represents 48% of the lake surface area. The underlying bedrock is composed of granites and syenites and is overlain by a thin layer of till. The catchment vegetation is comprised of Arctic species of mosses, grasses, and shrubs (Shemesh et al., 2001). There are two ephemeral inlets (max $6\,\text{cm}$ deep) in the eastern part of the lake and one outlet ($10\,\text{cm}$ deep) in the western part (Figure 1, Table S1). Besides streams, additional sources of water to rivers and lakes can be snow patches or inputs of groundwater (Pienitz et al., 2008). From mid-October until late May–early June, the lake is ice-covered. The catchment is snow-covered from mid-September to mid-June. In August, the lake is well-mixed, with no thermal stratification. The lake is classified as oligotrophic and has a pH of 6.8 and a dissolved organic carbon concentration of $2.3\,\text{mg}\,\text{l}^{-1}$ (Shemesh et al., 2001).

3 Numerical analyses – mass balance models

3.1 Radon mass balance

Radon (^{222}Rn, hereafter Rn) is produced from the radioactive decay of ^{226}Ra (Ra hereafter) present in rocks, soils, and sediments. Radon emanates from Ra bearing minerals, enters the groundwater, and is transported through the aquifer. Groundwaters usually contain Rn concentrations orders of magnitude higher than surface waters, and groundwater discharging into surface waters can thus be easily detected by a Rn enrichment with respect to surface waters (Burnett and Dulaiova, 2003).

Groundwater discharge into the Lake 850 was quantified using a Rn mass balance approach and assuming steady-state (Dimova and Burnett, 2011; Dimova et al., 2013). For steady-state conditions, the groundwater flow discharging into the lake can be determined by the imbalance between all Rn sources and loss terms (equation 1).

The sources of Rn are the main inlet streams ($n = 2$), Rn production by dissolved Ra in the water column, Rn diffusion from underlying sediments, and groundwater discharge. Radon losses include radioactive decay, atmospheric evasion, and losses through outlet streams ($n = 1$). Losses by recharge into underlying aquifers are considered minor, because the concentration of Rn seeping into sediments is usually much lower that seeping into the lake (Dimova and Burnett, 2011). By evaluating all Rn source and loss terms, the groundwater flow discharging into the lake can be determined using the following equation:

$$Q_{\text{gw}}Rn_{\text{gw}} + F_{\text{sed}}A + \lambda Ra_{\text{lake}}V + Q_{\text{in}}Rn_{\text{in}} = F_{\text{atm}}A + \lambda Rn_{\text{lake}}V + Q_{\text{out}}Rn_{\text{out}} \tag{1}$$

where Q_{gw} is the unknown groundwater discharge $[\text{m}^3\,\text{d}^{-1}]$; Q_{in} and Q_{out} are the discharge from inlet and outlet streams $[\text{m}^3\,\text{d}^{-1}]$, respectively; Rn_{lake} and Rn_{gw} are the concentrations of Rn $[\text{Bq}\,\text{m}^{-3}]$ in lake water and groundwater, respectively; Rn_{in} and Rn_{out} are the concentrations of Rn $[\text{Bq}\,\text{m}^{-3}]$ in the main inlet and outlet streams, respectively; Ra_{lake} is the concentration of Ra in lake water column $[\text{Bq}\,\text{m}^{-3}]$; F_{sed} is the net diffusive flux of Rn per unit area from lake sediments

[Bq m^{-2} d^{-1}]; F$_{atm}$ is the loss of Rn to the atmosphere [Bq m^{-2} d^{-1}]; λ is the radioactive decay constant of Rn [d^{-1}]; and A [m^2] and V [m^3] are the area and volume of the lake, respectively.

90   The calculation of Rn loss to the atmosphere was based on the empirical equation by MacIntyre et al. (1995):

$$F_{atm} = k(Rn_{lake} - \alpha Rn_{air}) \tag{2}$$

where k is the gas transfer coefficient [m d^{-1}] based on an empirical relationship that relates k with wind speed and lake area (Vachon and Prairie, 2013), and α is the air-water partitioning of Rn corrected for salinity and temperature (Schubert et al., 2012).

95   The steady-state assumption implies that Rn sources and Rn sinks are balanced and constant with respect to the timescale of Rn within the system. The residence time of Rn in the lake can be calculated by dividing the Rn inventory in the lake water by the sum of all tracer losses using the equation:

$$t_{Rn} \approx \frac{1}{\lambda + \frac{Q_{out}}{V} + \frac{k}{h}} \tag{3}$$

where λ is the radioactive decay constant of Rn [d^{-1}]; Q$_{out}$ is the discharge from outlet stream, V is the lake volume, k is the
100 gas transfer coefficient [m d^{-1}] based on an empirical relationship that relates k with wind speed and lake area (Vachon and Prairie, 2013) and h is the lake depth [m].

Groundwater discharges (Q$_{gw}$) were estimated for August and September 2019. For the remainder months, we interpolated the estimated values by assuming two different scenarios of i) constant or ii) variable groundwater inflows over the year (see Appendix A1) for variable groundwater inflows scenario).

105 **3.2 Water balance**

The lake water balance was calculated from the volumetric water balance equation:

$$\Delta V = Q_{in} + P + Q_{gw} - Q_{out} - E \tag{4}$$

where ΔV is the change in lake water volume, Q$_{in}$ and Q$_{out}$ are the stream inflow and outflow, respectively, Q$_{gw}$ is the groundwater inflow, P is precipitation, E is evaporation. Monthly summer precipitation of $48\,mm$ (ANS, 2020a) has been
110 considered to be included in the stream inflow term. Evaporation and precipitation have been shown to only have a small contribution to the lake water balance, and thus they are considered negligible here (Shemesh et al., 2001).

3.3 Silicon mass balance

The DSi flux into and from the lake is calculated as $\phi = Q \cdot c$, where Q is discharge [l s^{-1}] and c is DSi concentration [mg SiO$_2$ l^{-1}]. The DSi balance is then calculated as:

115 $$\Delta DSi = \phi_{in} + \phi_{gw} - \phi_{out} - \phi_{BSi} \tag{5}$$

where ΔDSi is the change of lake DSi [mg SiO$_2$ yr^{-1}], and ϕ_{in}, ϕ_{out} and ϕ_{gw} are the DSi fluxes of the inlet, outlet, and groundwater discharge [mg yr^{-1}], respectively. Finally, ϕ_{BSi} represents the flux of BSi into the sediment [mg SiO$_2$ yr^{-1}], and it was calculated as:

$$\phi_{\text{BSi}} = (\text{SAR} \cdot \rho_{\text{dry}} \cdot \text{BSiwt\%} \cdot \text{A}_{\text{sed}}) \cdot 1000, \tag{6}$$

120   where SAR is sediment accumulation rate [cm yr^{-1}] calculated from the age-depth model (see Methods section 4.1.2), ρ_{dry} is dry bulk sediment density [g cm^{-3}], BSiwt% is the mean of BSi content in sediments, A$_{\text{sed}}$ is the area of sedimentary basin of the lake [cm^2] and 1000 is the unit conversion from g to mg.

Assuming that the lake is in steady-state, which means that the sum of input DSi fluxes equals to the sum of output Si fluxes, thus ΔDSi = 0, DSi concentration in groundwater was then calculated by dividing ϕ_{gw} from Equation 5 by Q$_{\text{gw}}$. The

125   groundwater DSi flux in ice-free period is dependent on inlet (ϕ_{in}), outlet DSi flux (ϕ_{out}) and BSi flux to sediment (ϕ_{BSi}). However, during ice-covered period, the ϕ_{gw} is dependent only on ϕ_{BSi}, if there is some (scenario 1, Appendix B) and on differences of lake volume and DSi concentration. Thus, in order to solve Equation 5, ϕ_{BSi} and lake DSi concentration changes in ice-covered period are required. The ϕ_{gw} during ice covered period is calculated by a mixing model (see Appendix A2).

To constrain DSi concentrations in groundwater, we have examined 3 different scenarios considering different BSi fluxes

130   (ϕ_{BSi}) to the sediment driven by the length of diatom production. Two scenarios with maximal and minimal monthly BSi flux appear in the Appendix B aiming to describe maximal and minimal diatom production period and thus groundwater DSi concentrations. The scenario better describing recent diatom production considers that the diatom growing season and, thus, the BSi flux occurs in 4 months, from June until August, in a year (Shemesh et al., 2001), and that scenario is presented here.

3.4   Silicon isotope mass balance

135   The variability of the isotopic Si ratio of the lake water is likely to be biologically driven and, therefore, was described using a Si isotopic fractionation model. We hypothesize that the lake has sufficient inlet and groundwater supply to allow for DSi concentrations to remain high and that DSi is unlimited for diatom growth, thus, an open system model was used. The open system model (Varela et al., 2004) describes the expected diatom δ^{30}Si$_{\text{BSi}}$, as well as the post-uptake ratio of the lake water δ^{30}Si$_{\text{postuptake}}$.

140   $$\delta^{30}\text{Si}_{\text{BSi}} = \delta^{30}\text{Si}_{\text{initial}} + \varepsilon \cdot \text{f} \tag{7}$$

$$\delta^{30}\text{Si}_{\text{postuptake}} = \delta^{30}\text{Si}_{\text{initial}} - \varepsilon \cdot (1 - \text{f}) \tag{8}$$

where δ^{30}Si$_{\text{initial}}$ is the isotopic ratio of the initial DSi source, ε is the fractionation factor of freshwater diatoms $\smile 1.1 \pm 0.41$ ‰ (De La Rocha et al., 1997), and f is the fraction of remaining DSi calculated as $\text{f} = \frac{c_{\text{out}}}{c_{\text{initial}}}$, where c_{initial} and c_{out} are DSi concentrations before and after diatom production uptake. Thus, $(1 - \text{f})$ is the DSi utilization by diatom production. The initial

145   DSi concentration is calculated through mixing model with knowledge of the discharges (Q$_{\text{in}}$ and Q$_{\text{gw}}$) and DSi concentrations (c_{in} and c_{gw}) of the endmembers .

The initial isotopic ratio of lake DSi before diatom uptake is back calculated from $\delta^{30}\text{Si}_{\text{postuptake}}$ (Appendix A3). The known variables are the $(1-f)$ and the $\delta^{30}\text{Si}_{\text{postuptake}}$ represented either in the lake isotopic composition or in the lake outlet $\delta^{30}\text{Si}_{\text{out}}$, if $\delta^{30}\text{Si}_{\text{lake}} = \delta^{30}\text{Si}_{\text{out}}$. Further, the groundwater isotopic composition can be calculated from the initial isotopic Si mixture before diatom uptake and fractionation through isotope mixing model (see Appendix A3).

Similar to the Si mass balance, the isotope Si mass balance was examined through three scenarios that differ in BSi flux to the sediment representing different length of diatom production (Appendix B). As differences in BSi fluxes alter groundwater DSi concentrations, the isotopic composition is also changing. However, the scenario describing the recent lake functioning is used for the model presented here. Results of this model were compared with measured data of $\delta^{30}\text{Si}_{\text{BSi}}$ and $\delta^{30}\text{Si}_{\text{postuptake}}$ (which equals to $\delta^{30}\text{Si}_{\text{lake}}$). For validation, the groundwater $\delta^{30}\text{Si}_{\text{gw}}$ for monthly steady-state was calculated and compared with data in the literature.

4 Materials and Methods

4.1 Sample collection, chemical analyses and chronology

4.1.1 Water sampling

For DSi analyses, water samples from the ephemeral inlets and outlet streams, and lake waters were collected monthly from June to September 2019 (Figure 1, Table S1). Additionally, samples of two profiles of lake water from the deepest and a shallower part of the lake were collected in August and September 2019. All water samples were filtered directly in the field through a $0.45\,\mu\text{m}$ cellulose Sterivex™-HV Durapore filter and acidified with HCl to pH 2 in the laboratory. DSi concentrations were analyzed by the automated molybdate-blue method (Strickland and Parsons, 1972) with a Smartchem 200, AMS System™ discrete analyzer at Lund University with an instrumental error of $\pm 3.7\%$. All values for DSi concentrations are reported as mg of SiO_2.

For Rn analyses, surface water samples (maximum of $1.5\,\text{m}$ depth from the surface or $0.5\,\text{m}$ depth at the shallow depths) were collected from 5 different stations (Figure 1, Table S1). A deeper water sample ($4\,\text{m}$ depth) was collected from the central deeper point of the lake to evaluate the potential stratification of Rn concentrations. Samples of water from the main inlet and the outlet stream were also collected. Water samples were collected in $1.5\,\text{l}$ polyethylene terephthalate (PET) bottles with no headspace using a peristaltic pump. Water was pumped directly into the bottle and left overflowing to replenish the volume at least three times to ensure minimal contact with air. Shortly after collection, Rn concentrations were determined using a Rn-in-air alpha spectrometer RAD7 (Durridge Inc.) coupled to the Big Bottle RAD H_2O accessory (Durridge Inc.). All Rn concentrations were decay corrected for the time of collection.

Discharges from the inlet and outlet streams were determined by measuring the water velocity at 60% of the sampling point depth using the six-tenths-depth method (Turnipseed and Sauer, 2010) and creating a cross section through the tributary.

4.1.2 Sediment sampling

Two short ($\sim 15\,\mathrm{cm}$) sediment gravity cores were sampled with a HTH gravity corer in March and August 2019 (Table S1). Both cores showed an undisturbed water-sediment interface. One of the cores was sliced directly in the field in $1\,\mathrm{cm}$ sections. Each section was weighed before and after freeze drying to determine water content, porosity, and wet and dry bulk densities. Total organic carbon (TOC) and total nitrogen (TN) analyses were carried out on all freeze dried samples, after packing $5\,\mathrm{to}$ $10\,\mathrm{mg}$ of dry sediment into tin capsules. Five samples throughout the core were tested for carbonate content by acidifying with HCl and heating to $60\,^\circ\mathrm{C}$ before the TOC measurements (Brodie et al., 2011). The measurements were done on a COSTECH ECS4010 elemental analyzer at the Department of Geology, Lund University, with the mean analytical uncertainty for TOC of $0.3\,\mathrm{wt\%}$ based on duplicate analysis ($n = 14$). The carbonate content calculated as a difference in TOC between de-calcified and bulk sample was below $0.5\,\mathrm{wt\%}$, thus considered negligible.

Biogenic SiO_2 content in the sediment was analyzed by sequential alkaline extraction (Conley and Schelske, 2001). Freeze dried and homogenized samples were digested in $0.1\,\mathrm{M\,Na_2CO_3}$ (sample reagent ratio $0.03/40\,\mathrm{[g/ml]}$) in a shaking bath at $85\,^\circ\mathrm{C}$ for 5 hours. Subsamples of $100\,\mu l$ were taken at 3, 4, and 5 hours and neutralized in $9.9\,\mathrm{ml}$ of HCl to examine for the dissolution of minerals. The extracted DSi was measured using the automated molybdate-blue method (Strickland and Parsons, 1972) with a Smartchem 200, AMS System™ discrete analyzer at Lund University with an instrumental error of $\pm 3.7\%$. As there were no changes in the amount of total Si extracted during the time course of dissolution ($n = 3$, slope ≈ 0), the mean BSi concentration from all the values was used to estimate BSi concentration with no correction applied for Si-containing minerals (Conley, 1998). All values for BSi concentrations are reported wt% of SiO_2.

All sediment samples were analyzed for radionuclide concentrations (^{210}Pb, [226]Ra, and ^{137}Cs) at Lund University. [210]Pb, [226]Ra, and ^{137}Cs were determined by direct γ-counting using a high-purity germanium detector ORTEC (Model GEM FX8530P4-RB). Freeze-dried and ground samples were sealed for at least 3 weeks before counting to ensure secular equilibrium of [226]Ra daughters. [210]Pb was determined through the $46\,\mathrm{keV}$ γ-emission and [226]Ra through the 351 and $609\,\mathrm{keV}$ γ-emission of its daughter nuclide [214]Pb and [214]Bi, respectively. [137]Cs was measured by its emission at $662\,\mathrm{keV}$. Self-absorption was measured directly, and the detector efficiency was determined by counting a National Institute of Standards and Technology sediment standard.

Sediment core chronologies were obtained by applying the Bayesian statistics approach with software package Plum (Aquino-López et al., 2018). The Plum package was applied using the default settings for the thickness of Bacon sections ($1\,\mathrm{cm}$). Plum used the individual [226]Ra measurements as an estimate of the supported ^{210}Pb concentration. The unsupported ^{210}Pb was found in upper most $7\,\mathrm{cm}$, and the software package Plum (Aquino-López et al., 2018) extrapolated the ages for the remaining $7\,\mathrm{cm}$ based on measured data.

To constrain the Rn mass balance, the second sediment gravity core was used for equilibration experiments in order to determine Rn diffusion from underlying sediments and the Rn concentration representative of the groundwater discharging into the lake. Briefly, diffusive flux experiments were carried out in the laboratory by incubating $\sim 200\,\mathrm{g}$ of dry sediment placed into $500\,\mathrm{ml}$ PET bottles with Milli-Q® water, as described in Chanyotha et al. (2014). Using the RAD7 coupled to the

Big Bottle RAD H$_2$O accessory (Durridge Inc.), Rn concentrations were monitored for 14 hours. The rate of Rn diffusion from the sediment (F$_{diff}$) was derived from the exponential ingrowth of Rn concentrations with time. The bottles containing grab sediments were then stored for more than a month and periodically shaken. After this time, the Rn concentration in water was measured using the RAD7 and converted into groundwater endmember activities using porosity and bulk density as described in Chanyotha et al. (2014).

4.2 Stable Si isotopes analyses

Stable Si isotope analyses were performed on diatoms recovered from sediment, lake, and stream water samples. Cleaned diatom material ($n = 3$) from a published core taken in 1999 (Shemesh et al., 2001) was used to determine the stable silicon isotope ratio in sedimentary diatoms and then used in mass balance models. Briefly, pure diatom samples ($\sim 0.8\,\text{mg}$) were digested with 0.5 to 1 ml of 0.4 M NaOH (analytical purity) at 50 °C for at least 48 hours. When all diatoms were dissolved, samples were diluted with Milli-Q® water to prevent precipitation and fractionation of amorphous silica, then neutralized by 0.5 to 1 ml of 0.4 M suprapur® HCl. The solutions were measured for their DSi concentration to obtain the Si recovery, which was between 90 and 100%. Sample solutions were purified for Si isotope analysis by cation-chromatographic separation using 1.5 ml cation-exchange DOWEX® 50W-X8 (200-400 mesh) resin following the method of Georg et al. (2006). Silicon from filtered water samples was purified using the same cation-exchange method (Georg et al., 2006). The international Si standard NIST reference material RM-8546 (former NBS-28) and laboratory standard Diatomite were prepared by alkaline NaOH fusion and purified following protocol by Georg et al. (2006).

The reference material RM-8546 (former NBS-28) and laboratory standards IRMM-018, Big-Batch, and Diatomite used in the Vegacenter, Swedish Museum of Natural History, Stockholm were prepared by another type of fusion with LiBO$_2$ (Sun et al., 2010). Thus, our alkaline NaOH fused NBS-28 and Diatomite standards (Georg et al., 2006), purified in identical way as the samples, were matrix matched to contain $3\,\text{mg}\,\text{l}^{-1}$ Li IPC-MS standard. Similarly, all purified samples were diluted to a concentration of $3\,\text{mg}\,\text{l}^{-1}$ of Si in 0.12 M SeaStar™ HCl matrix and doped with Li to contain $3\,\text{mg}\,\text{l}^{-1}$ Li to match the standard matrix.

The stable isotope measurements were carried out on a NuPlasma (II) HR multi-collector inductively conducted plasma mass spectrometry (MC-ICP-MS, Nu Instruments™) with an Apex HF desolvation nebulizer at the Vegacenter. The ^{28}Si signal intensity of full procedural blanks was determined to be less than 0.35% of the total signal intensity, thus no sample contamination was observed. Silicon isotope data are reported as deviations of $\frac{^{30}\text{Si}}{^{28}\text{Si}}$ and $\frac{^{29}\text{Si}}{^{28}\text{Si}}$ from the NBS-28 reference solution in ‰, denoted δ^{30}Si and δ^{29}Si as follows:

$$\delta^{30}\text{Si} = \left(\frac{\frac{^{30}\text{Si}}{^{28}\text{Si}}\,\text{sample}}{\frac{^{30}\text{Si}}{^{28}\text{Si}}\,\text{NBS28}} - 1 \right) \cdot 1000. \tag{9}$$

Each sample was measured three times, bracketed by NBS-28 in between, and full chemical replicates for diatom ($n = 3$) and water samples ($n = 23$) were measured for 65% of all samples (total measurements $n = 137$). Secondary reference materials Diatomite, Big-Batch, and IRMM-018 were measured throughout all measuring sessions in a period of 3 years, with means of

$\delta^{30}\mathrm{Si} = 1.26 \pm 0.19\,\text{‰}$ $(2\mathrm{SD}_{\mathrm{repeated}}, n = 219)$ for Diatomite, $\delta^{30}\mathrm{Si} = -10.64 \pm 0.18\text{‰}$ $(2\mathrm{SD}_{\mathrm{repeated}}, n = 77)$ for Big-Batch, and $\delta^{30}\mathrm{Si} = -1.77 \pm 0.18\text{‰}$ $(2\mathrm{SD}_{\mathrm{repeated}}, n = 100)$ for IRMM-018 for quality control purposes. All secondary reference material values were in good agreement with values from a previous interlaboratory comparison (Reynolds et al., 2007). The reproducibility of all samples was $< 0.2\,\text{‰}$. At the Vegacenter, the long-term precision for $\delta^{30}\mathrm{Si}$ is 0.15‰ (2SD).

5 Results

5.1 Lake water chemical and isotopic properties

Lake 850 is a subarctic lake in a region with strong seasonality. The discharge from inlets and the outlet streams show a decreasing trend throughout the ice-free period from June through September (Table 1). The highest water flow rates are observed during the snowmelt period (June and July). Inflow from the stream inlets to the lake in August is low, and both inlets are dry in September.

During the ice-free period direct surface precipitation is $0.65\,\mathrm{l\,s^{-1}}$, which represents only 1.4% of the lake volume and similar or higher discharges are observed in the stream inlets from July to August. Therefore, the influence of precipitation on the water mass balance is limited. The calculated lake water residence time during the high-flow regime in June, defined as lake volume $(1.2 \cdot 10^5\,\mathrm{m^3})$ divided by the lake outlet discharge (Table 1), is 65 days. During the rest of the year, the lake water residence time is between 5 months and 2.4 years.

Lake DSi concentration varies seasonally (Table 1), with the highest values during the ice-covered period in March, reaching $2.51 \pm 0.35\,\mathrm{mg\,SiO_2\,l^{-1}}$. With snowmelt, the lake DSi decreases to $1.24 \pm 0.02\,\mathrm{mg\,SiO_2\,l^{-1}}$ in June and to its minimum value of $0.96 \pm 0.06\,\mathrm{mg\,SiO_2\,l^{-1}}$ in August. With the first snow in September, lake DSi concentration rebounds, having values of $1.37 \pm 0.04\,\mathrm{mg\,SiO_2\,l^{-1}}$. Data of DSi for the inlets and the outlet streams show two different patterns during the year (Table 1). A lower inlet DSi concentration of $2.34 \pm 0.05\,\mathrm{mg\,SiO_2\,l^{-1}}$ is observed during snow melt in June compared to July and August, when the inlet DSi concentrations increase to $4.79 \pm 0.05\,\mathrm{mg\,SiO_2\,l^{-1}}$ and $5.05 \pm 0.12\,\mathrm{mg\,SiO_2\,l^{-1}}$, respectively. The lake outlet DSi concentration shows little variability, with the lowest concentration of $0.94 \pm 0.01\,\mathrm{mg\,SiO_2\,l^{-1}}$ in July and only a small increase up to $1.12 \pm 0.03\,\mathrm{mg\,SiO_2\,l^{-1}}$ towards the end of the summer season in August. In September, when the inlet streams are snow covered, the DSi concentration in the outlet stream is the same as the lake water concentration at $1.37 \pm 0.01\,\mathrm{mg\,SiO_2\,l^{-1}}$.

The stable Si isotope ratios of the lake, inlet, and outlet streams vary during the year. The heaviest lake $\delta^{30}\mathrm{Si}_{\mathrm{lake}}$ ratio, $1.27 \pm 0.15\text{‰}$, is observed during the ice-cover period, and the lightest ratio, $0.73 \pm 0.10\text{‰}$, occurs during the snowmelt in June (Table 1). In June, the inlet has a lighter $\delta^{30}\mathrm{Si}_{\mathrm{in}}$ of $0.02 \pm 0.10\text{‰}$, whereas in August the inlet isotopic ratio $0.78 \pm 0.15\text{‰}$ has similar values as the lake. The $\delta^{30}\mathrm{Si}_{\mathrm{out}}$ of the outlet in June is slightly heavier $(0.89 \pm 0.10\text{‰})$ compared to the lake $\delta^{30}\mathrm{Si}_{\mathrm{lake}}$. In July the outlet $\delta^{30}\mathrm{Si}_{\mathrm{out}}$ is lighter than the inlet one (Table 1). During the remainder of the year, the outlet $\delta^{30}\mathrm{Si}_{\mathrm{out}}$ is closely similar to the lake and inlet $\delta^{30}\mathrm{Si}_{\mathrm{lake}}$.

5.2 Groundwater discharge

Surface lake Rn concentrations range between $94\,\mathrm{Bq\,m^{-3}}$ to $136\,\mathrm{Bq\,m^{-3}}$ in August and from $96\,\mathrm{Bq\,m^{-3}}$ to $126\,\mathrm{Bq\,m^{-3}}$ in September. Dissolved Ra in lake waters is assumed to be similar to those found in other lakes in the region ($1.4\pm0.6\,\mathrm{Bq\,m^{-3}}$). However, the measured Rn inputs (the stream inlets) due to Ra decay were below 0.5%, compared to the net excess of Rn delivered by groundwater discharge. Thus, the inlet Rn flux was neglected in the total Rn balance.

There was no significant vertical stratification of Rn concentration with Rn concentrations in deep waters (105 ± 26 and $79\pm24\,\mathrm{Bq\,m^{-3}}$) in August and September, respectively. Equation 1 was solved analytically to obtain the amount of groundwater discharging into the lake (Q_{gw}) in August and September 2019. Uncertainties of individual terms were included in the estimation of the associated uncertainty (NORM, 1995; Taylor and Kuyatt, 1994).

Using the mean wind-speed for $48\,\mathrm{h}$ period prior sampling (3.1 ± 1.2 and $5.0\pm1.8\,\mathrm{m\,s^{-1}}$ in August and September, respectively) resulted in k_{Rn} estimates of 1.1 ± 0.2 and $1.2\pm0.4\,\mathrm{m\,s^{-1}}$. Uncertainties include the variation of wind speed and uncertainties associated with the empirical equation to estimate k_{Rn}. Using the Rn concentration in lake waters, total losses of Rn to the atmosphere are 123 ± 32 and $138\pm32\,\mathrm{Bq\,m^{-2}\,d^{-1}}$ in August and September, respectively. Radon losses due to decay were 125 ± 22 and $123\pm15\,\mathrm{Bq\,m^{-2}\,d^{-1}}$, respectively, where uncertainties are obtained from the analytical uncertainties for Rn concentrations in lake waters. Losses of Rn through the outlet stream were 7 ± 4 and $9\pm4\,\mathrm{Bq\,m^{-2}\,d^{-1}}$. Among all Rn losses, atmospheric evasion (50%) and decay (47%) were the terms that have the largest contribution to the Rn mass balance. Radon losses through the outlet stream are almost negligible (3%). Additionally, using the average k_{Rn} and Q_{out} (equation 3), the average ^{222}Rn residence time in Lake 850 is ~ 2 days.

Diffusive Rn flux from underlying sediments (F_{diff}) obtained from diffusion experiments in the lab is $89\pm17\,\mathrm{Bq\,m^{-2}\,d^{-1}}$, and it is one of the main sources of Rn into the system. Fluxes of Rn from the sediment compensate for up to 57% of total Rn losses. Uncertainties associated with this flux are from analytical uncertainties in the slope for the regression analyses of the increase in Rn concentration through time in the sediment diffusion experiment. Due to the low concentrations of Ra in lakes from the same area ($1.4\pm0.6\,\mathrm{Bq\,m^{-3}}$, *C. Olid, unpublished data*), Rn inputs due to Ra decay were considered negligible in the Rn mass balance.

Rn inputs from groundwater are required to balance the Rn losses from the lake. The Rn flux into the lake through groundwater discharge is calculated to be $164\pm51\,\mathrm{Bq\,m^{-2}\,d^{-1}}$ and $178\pm39\,\mathrm{Bq\,m^{-2}\,d^{-1}}$ in August and September, respectively. Considering the lake area of $20\,000\,\mathrm{m^2}$ and the Rn concentration in groundwater obtained from incubation experiments ($10626\pm1720\,\mathrm{Bq\,m^{-3}}$), groundwater fluxes are $3.58\pm1.11\,\mathrm{l\,s^{-1}}$ and $3.88\pm0.86\,\mathrm{l\,s^{-1}}$ for August and September, respectively. Note that this is a conservative estimate for groundwater fluxes, because we use the highest measured Rn concentration as the endmember.

Due to the lack of Rn measurements for the entire year, we estimated groundwater inputs for the months where no sampling was carried out using two scenarios: (i) constant groundwater inflow of $3.73\pm1.40\,\mathrm{l\,s^{-1}}$, calculated as the mean of the August and September data; and (ii) modelled groundwater inflow based on groundwater fluxes obtained from a lake survey in the Abisko region in 2018–2019 (*C. Olid, unpublished data*), which ranged from $2.28\pm0.50\,\mathrm{l\,s^{-1}}$ to $7.69\pm1.70\,\mathrm{l\,s^{-1}}$ (Figure 2).

The annual Rn fluxes follow a pattern of a distinct peak in discharge in June and a gradual decrease towards July – October, reaching the base-flow level in November (Figure 2). The ratio between the groundwater Rn flux in September in Lake 850 and the groundwater Rn fluxes from the lake survey was used to model the missing groundwater Rn fluxes in Lake 850 (Figure 2, Appendix A1).

5.3 Age-depth model, lithology and mass accumulation rates

The age-depth model for the sediment core is shown in Figure 3. The mean sediment accumulation rate (SAR) was estimated to be $0.083 \pm 0.041 \, \text{cm} \, \text{yr}^{-1}$, which equals a sediment accumulation rate of $12 \pm 6 \, \text{yr} \, \text{cm}^{-1}$ and a mass accumulation rate (MAR) of $16.0 \pm 9.3 \, \text{mg} \, \text{cm}^{-2} \, \text{yr}^{-1}$. The presence of mosses in the sediment was observed during the core processing and also was described in the sediment lithology by Shemesh et al. (2001). Changes in the sediment content of aquatic or terrestrial mosses, was also supported by the C/N wt% ratio (Figure 4), suggesting this is the cause of changes in MAR.

Lake 850 sediment is composed of carbonate-free clay gyttja with a mean TOC content of 11.4 wt%, mean TN of 1.1 wt%, and a resultant C/N wt% ratio of 10.2 (Figure 4). Sediment porosity as high as 89.5% is found in the surface sediment, where sediment dry bulk density mean is $0.19 \pm 0.06 \, \text{g} \, \text{cm}^{-3}$. The BSi concentration along the sediment varies from 13.2 ± 0.28 wt% to 22.8 ± 0.24 wt%, with the highest BSi concentration in the surface of the core. The BSi concentrations reported here are lower than previous measurements. For example, BSi concentration in the surface sediment of Lake 850 was previously reported to be 40.3 wt% (Rosén et al., 2010), which is twice the value found here, demonstrating a high variability of BSi in the sediments.

From MAR and BSi wt% we estimated the BSi accumulation rate (ϕ_{BSi}). BSi accumulation rates show stable values around $1.8 \, \text{mg} \, \text{SiO}_2 \, \text{cm}^{-2} \, \text{yr}^{-1}$ in the upper $7 \, \text{cm}$ of the core, whereas an increase in BSi accumulation is observed towards the bottom $7 \, \text{cm}$ of the core (Figure 4) likely connected to the higher MAR. The mean BSi accumulation rate for the entire gravity core of $2.9 \pm 1.5 \, \text{mg} \, \text{SiO}_2 \, \text{cm}^{-2} \, \text{yr}^{-1}$ was used as the BSi flux to sediment in the mass balance models. The mean diatom isotopic ratio ($\delta^{30}\text{Si}_{\text{BSi}}$) measured on cleaned diatoms from the upper most $8 \, \text{cm}$ of sediment piston core from 1999 (Shemesh et al., 2001) is $0.07 \pm 0.43 \, \text{‰} \, (n = 3)$.

6   Mass balance models

6.1   Water balance

Two water balance scenarios were considered where changes in the lake level were evaluated: (i) constant groundwater inflow over the annual cycle as an additional water source, and (ii) modelled groundwater discharges varying throughout an annual cycle (Figure 5 and A1). In both scenarios, lake-level increases during the ice-covered period (Figure 5, blue and green line) are a result of a potential groundwater inflow. This accumulated water is released through the outlet when the lake ice starts to melt in May-June, and the outlet discharge is thus high (Table 1). After this period, lake-level is stabilized and groundwater replenishes the lake original volume during short periods over the summer.

When groundwater discharge is assumed to be constant (Scenario i, $3.73 \pm 1.40\,\mathrm{l\,s^{-1}}$) based on our data from August and September, the lake shows annual lake-level changes up to $1.9\,\mathrm{m}$ (Figure 5 and A1, blue line). From July to December, the lake volume is restored by the groundwater inflow, and, on the annual time scale, the lake-level would increase around $2\,\mathrm{m}$ every year (Figure 5, blue line).

Using the modelled annual groundwater inflow (Scenario ii, Figure 2), limited lake-level changes were observed. The maximum lake-level decrease is $1.4\,\mathrm{m}$ during summer (Figure 5 and A1, green line), but groundwater discharge restores lake-level during upcoming months. Taking into account the uncertainties, lake-level variation can be as great as $2.8\,\mathrm{m}$ or none (Figure 5 and A1, green shading). This scenario with the smallest lake-level changes is in agreement with previous results of oxygen isotopes mass balance (Shemesh et al., 2001). Therefore, we used this water balance model further for the Si balances.

6.2 Silicon and Silicon isotope mass balance

Based on the steady-state assumption, BSi accumulation occurs in conditions when the total DSi influx is higher that the stream DSi outflux. Therefore, we construct a Si mass balance based on stream inlets and the outlet. The DSi influx through the inlet stream is not sufficient to maintain lake DSi concentration at steady-state in June (red and blue triangles, Figure 6A). In contrast, in July and August sufficient DSi enters the lake to supply the outlet DSi flux. The monthly inlet DSi flux is between 0.22 ± 0.11 to $0.62 \pm 0.31\,\mathrm{kg}\ \mathrm{SiO_2}\ \mathrm{day^{-1}}$, while the outlet DSi flux ranges from 0.19 ± 0.10 to $2.21 \pm 1.11\,\mathrm{kg}\ \mathrm{SiO_2}\ \mathrm{day^{-1}}$. However, diatom production is an additional sink of Si by creating a BSi flux into the sediment. The DSi influx is, thus, not sufficient to account for both the DSi outflux and the BSi flux into the sediment (Figure 6A). Therefore, an external source (i.e., groundwater discharge) must supply additional DSi to compensate for the mean BSi flux ($2.9\,\mathrm{mg}\ \mathrm{SiO_2}\ \mathrm{cm^{-2}}\ \mathrm{yr^{-1}}$) into the sediment.

Groundwater discharges from scenario ii (Figure 2) were used to build a Si mass balance and a Si isotope mass balance. Here, we assume that the recent BSi flux into the sediment occurs only during the diatom growing season (from June until September) (Figure 6A; Shemesh et al., 2001). The missing DSi flux resulting from the mass balance was considered to originate from the groundwater flux, and thus, we use this flux to calculate back the groundwater DSi concentration and isotopic ratio.

During the diatom growing season, the modelled BSi flux into the sediment increases up to $1.76 \pm 0.87\,\mathrm{kg}\ \mathrm{SiO_2}\ \mathrm{day^{-1}}$ (magenta line, Figure 6A), which produces DSi deficiency in the lake. To balance this deficiency, groundwater discharge must supply between 1.62 ± 1.21 and $3.39 \pm 1.81\,\mathrm{kg}\ \mathrm{SiO_2}\ \mathrm{day^{-1}}$ during the diatom growing season (cyan line, Figure 6A). Considering the modelled groundwater discharges derived from Rn mass balance, the DSi concentration in the groundwater is estimated to range from $3.96 \pm 2.14\,\mathrm{mg}\ \mathrm{SiO_2}\,\mathrm{l^{-1}}$ to $5.85 \pm 2.99\,\mathrm{mg}\ \mathrm{SiO_2}\,\mathrm{l^{-1}}$ during diatom growth (cyan line, Figure 6B). During the ice-covered period the BSi flux into the sediment is considered to be negligible, while groundwater is still flowing into the lake. The winter groundwater concentration is calculated from the difference in the lake concentration from September ($1.02 \pm 0.91\,\mathrm{mg}\ \mathrm{SiO_2}\,\mathrm{l^{-1}}$) to March ($2.51 \pm 0.35\,\mathrm{mg}\ \mathrm{SiO_2}\,\mathrm{l^{-1}}$) (Appendix A2). Therefore, the groundwater discharging into the lake from late-October until mid-June is the only water inflow with a DSi concentration of $5.50 \pm 1.22\,\mathrm{mg}\ \mathrm{SiO_2}\,\mathrm{l^{-1}}$.

The Si isotopes mass balance using the open fractionation model (Varela et al., 2004) shows that the higher demand of DSi in the productive months (Figure 6A, B) needs to have a lighter isotopic composition in order to produce the $\delta^{30}\mathrm{Si_{BSi}}$ of

$0.07 \pm 0.43‰$ measured on diatoms preserved in the sediment. The isotopically lighter source is assumed to be groundwater discharge, with calculated ranges from $-0.55 \pm 0.55‰$ in July to $0.25 \pm 0.58‰$ in September (Figure 6C). Using the modelled groundwater δ^{30}Si, the expected δ^{30}Si$_{BSi}$ in all productive months varies from $-0.49 \pm 0.49‰$ to $-0.01 \pm 0.56‰$ (not shown), values that are in agreement with the sediment BSi of δ^{30}Si$_{BSi} = 0.07 \pm 0.43‰$. The production consumes 73% of the initial DSi in June, 77% in July and September, and 79% in August. During the ice-covered period from late-October until mid-June, the groundwater base flow is considered to be constant, calculated from the difference of the lake isotopic ratios from September until March (Appendix A3), and thus the δ^{30}Si$_{gw} = 1.43 \pm 0.82‰$ (Figure 6C).

7 Discussion

Lake 850 is unusual in terms of both the DSi and BSi concentration in water and sediment, respectively. The maximum DSi concentration of $2.51 \, \text{mg SiO}_2 \, \text{l}^{-1}$ in March is among the top 10% of lakes in Northern Sweden (Bigler and Hall, 2002). The mean BSi content in the lake sediment of 40 wt% (Rosén et al., 2010) places Lake 850 in the upper 6% of lake sediments studied worldwide (Frings et al., 2014). Based on the positive correlation between water residence time and the relative retention of DSi in lakes (Frings et al., 2014), Lake 850 with its DSi retention of 35±17% of the total DSi inlet input and a residence time ranging from 0.18 to 2.4 years, accumulates more DSi as BSi than expected. Although several factors, including the morphology of the watershed (Jenny, 1941; Rubensdotter and Rosqvist, 2003), diatom production and low detrital input (Conger, 1942), vegetation (Struyf et al., 2010), and preservation potential (Ryves et al., 2003) are known to affect sedimentation regimes and BSi accumulation resulting in a diatom-rich sediment, we show here that groundwater input is an important factor leading to the high BSi accumulation in Lake 850.

The combined results from the water, Rn, and Si mass balances indicated the importance of an external source of DSi through groundwater discharge. Groundwater inflow was the primary water and DSi supply to the lake, with a contribution about 3 times higher than the stream inlets (Figure 6A). The Si and Si isotope mass balance models showed that groundwater DSi concentration and isotopic composition varied during the ice-free period, compared to the ice-covered period, when they were stable (Figure 6B, C).

The significance of groundwater-sourced DSi to the lake's Si cycle is also evidenced by the relatively lighter stable Si isotope ratio of diatoms from sediment, which suggests that groundwater is the primary DSi source for diatoms. Stream inputs could also be a source of DSi for diatoms, especially in early spring, when snowmelt can deliver isotopically lighter DSi by displacement of shallow groundwater into the stream inlet (Campbell et al., 1995). However, spring snowmelt water and groundwater in June are likely to have the same isotopic composition (Figure 6C) because the same factors, e.g., short residence time in the watershed are present in both types of water. Thus, only by using mass balance is the quantification of each DSi source apparent, providing evidence that groundwater supplies almost 4 times more DSi compared to streamflow in June. Our results suggest that the groundwater supply plays a crucial role in providing DSi for the production of diatoms and accumulation of BSi in Lake 850.

7.1 Environmental controls on BSi accumulation

The results from our study can be applied more broadly to other lakes to evaluate factors governing the accumulation of diatom-rich sediment. BSi-rich sediments are likely to be found in lakes situated on silica-rich bedrock, such as in Lake Challa, Tanzania/Kenya (Barker et al., 2013), or, as shown here, in lakes with sufficient DSi inputs from groundwater that supply sufficient DSi during the diatom growing season to alleviate potential DSi limitation of diatom growth. In addition, lakes with high autochthonous carbon production and deposition combined with very low mean sedimentation rates, which commonly characterize Arctic lake sediments (Wolfe et al., 2004), as well as lakes with low-relief watershed morphology and with low stream input, which combined yield low quantities of fine-grained clastic input, are potential systems for high BSi accumulation (Conger, 1942).

7.2 The role of groundwater in the water balance

The water balance coupled with the Rn mass balance indicated that groundwater discharge is an essential water source for the lake. Both models of groundwater inflow (constant and varying groundwater inputs) demonstrated changes in lake volume as a result of high-water discharge at the outlet of the lake during spring snowmelt. More pronounced changes in lake volume were observed in scenario i, where constant groundwater inflow was assumed (Figure 5, blue line). However, because the oxygen isotope data showed negligible evaporation and precipitation effect on lake volume change (Shemesh et al., 2001), this model is not considered to be the most realistic. Scenario ii, which considered a variable groundwater flow (Figure 5, green line) seems to be more realistic. The modelled groundwater hydrograph (Figure 2) is comparable with the hydrograph of the neighboring river Miellejokha (Figure S1) and resembles the hydrographs of groundwater discharge in studies of high-altitude lakes from other regions (Clow et al., 2003; Hood et al., 2006; Huth et al., 2004; Liu et al., 2004). The results from this model show that groundwater discharge is up to 5 times higher than the lake water outflow through the outlet. Similarly, groundwater discharge brings from 3 to 17% of the lake volume depending on the month.

7.3 The role of groundwater in Si concentration mass balance and Si isotope mass balance

The lake Si mass balance (Figure 6A) shows that modelled groundwater concentration and flux of BSi vary through the year, which is similar to observations from Crystal Lake in Wisconsin (Hurley et al., 1985). Seasonal variations in groundwater DSi concentration related to discharges were also observed in Canadian rivers with groundwater inputs (Maavara et al., 2018). Moreover, the calculated BSi flux into the sediment is comparable (or higher) with BSi fluxes observed in some of the North American Great Lakes (Conley, 1988; Newberry and Schelske, 1986; Schelske, 1985) and lakes with diatomaceous sediment in the Arctic (McKay et al., 2008; Kaplan et al., 2002; Tallberg et al., 2015).

The model of stable Si isotopes shows little variation during the ice-covered period, as no diatom production is expected. The modelled δ^{30}Si of groundwater for the ice-covered period (Figure 6C) falls into the range of measured groundwater isotopic composition worldwide, which ranges from -1.5 to 2‰ (Frings et al., 2016). However, the modelled groundwater ratio δ^{30}Si$_{gw}$ is heavier than found in other groundwater studies (Georg et al., 2009; Opfergelt et al., 2011; Ziegler et al.,

2005), which may reflect lower dissolution of primary minerals, longer groundwater residence time, and possibly some clay mineral formation in the groundwater pathway (Frings et al., 2016; Pokrovsky et al., 2013) during the ice-covered period. Further, no diatom production, and thus no associated Si isotope fractionation, is expected in winter. Therefore, the $\delta^{30}Si_{lake}$ is influenced by the input of $\delta^{30}Si_{gw}$ only and not by diatom production. The $\delta^{30}Si_{lake}$ measured in March is slightly lighter than all modelled $\delta^{30}Si_{gw}$ for the ice-covered period, which can be explained by diatom dissolution in the uppermost sediment layers. However, if the uncertainties of the modelled groundwater isotopic composition are taken into account, the lake ratio is within the same range as the groundwater ratio. Therefore, no additional processes must be present during the ice-covered period, and the groundwater isotopic ratio is reflected in the lake isotopic signal. With snowmelt, the decrease of the modelled $\delta^{30}Si_{gw}$ reflects the increase in weathering of primary minerals and decrease in the groundwater residence time due to higher discharges, as also observed in Arctic rivers (Pokrovsky et al., 2013).

The greatest variation in the isotopic ratio of groundwater occurs in August, when the modelled groundwater isotopic composition is fully dependent on the changes in BSi flux into the sediment. As the yearly BSi accumulation occurs during the diatom growing season which is only 4 month, the modelled groundwater must bring additional DSi to supply diatom production. Hence, the isotopic model calculating the groundwater isotopic composition shows $\delta^{30}Si_{gw}$ comparable with values for groundwater reported in the small number of other studies (Frings et al., 2016; Opfergelt et al., 2011). Further, the calculated $\delta^{30}Si_{BSi}$ based on the initial mixture of the modelled groundwater and stream inlet ratio gives results within the range of the measured $\delta^{30}Si_{BSi}$.

7.4 Model uncertainties

The largest sources of uncertainty in the water and silicon balance models (Figure 5, SA1 and 6) are the discharge uncertainties of the inlet and outlet and the winter groundwater discharges. The spring snowmelt is dynamically changing the inlet and outlet discharges, as has been observed on rivers in the area, such as Miellejohka (Figure S1). With only a single sample every month, there is no information on variation of the stream on a finer temporal scale. Thus, monthly stream flow and the modelled groundwater discharges might be over- or underestimated. Further, uncertainties in the isotopic model and the isotopic composition of the groundwater were propagated from the mass balance model and from the stable isotopic measurements, especially in the outlet water in August.

The water balance based on modelled groundwater inflow suggests that lake-level changes throughout the year are within a range of 0 to $1.4\,\mathrm{m}$ (Figure 5, green line), and, thus, lake area and mean depth also vary throughout the year. Therefore, the underlying assumptions of constant depth and area are likely overestimating lake-level change. For a more precise model of lake-level, lake volume variations and a detailed bathymetry of Lake 850 are needed. However, the importance of the groundwater contribution to Lake 850 supports the evidence that groundwater should be considered as an important water and DSi source for high-altitude and high-latitude lakes, with support of data on groundwater DSi in Lake O'Hara (Hood et al., 2006), Lake Myvatn (Opfergelt et al., 2011) and Crystal Lake (Hurley et al., 1985; Kenoyer and Anderson, 1989).

Another source of uncertainties in the Si and Si isotope mass balance models originates from the uncertainties on the age-depth model. The uncertainties on MAR, which are calculated from the SAR and the densities are as high as 50%. It is

likely due to changes in the sediment composition and increased content of mosses. Therefore, the BSi flux to the sediment carries similar or higher uncertainty. As a result of those uncertainties, the modelled groundwater concentrations and isotopic composition are ranging greatly.

Additionally, the diatom preservation efficiency, which is globally around 3% in the oceans (Treguer et al., 1995), and, in deep lakes around $1-2\%$ (Ryves et al., 2003) of the total diatom production, suggests that $97-99\%$ of diatom BSi is redissolved in the water column in those environments. However, no estimates of sediment preservation efficiency are available for small, cold lakes such as Lake 850. Therefore, the mass balance can be slightly underestimated, in case that the BSi flux into the sediment, which was calculated from the sediment record represents only a fraction of the total production. To eliminate this source of uncertainty annual monitoring of diatom production and accumulation would be needed.

Uncertainty also results from the variability among sediment cores in their BSi content. BSi concentrations in the sediment vary from 13 to 40 wt% in different cores (this study; Rosén et al., 2010). We have tested the combination of the MAR ($16.0\,\mathrm{mg\,cm^{-2}\,yr^{-1}}$) reported from this study with the highest BSi of 40.3 wt% from a companion core from Lake 850 (Rosén et al., 2010) to evaluate the impact of BSi flux on the groundwater concentrations. The yearly BSi flux would need to increase 2.2 times, which would result in 1.3 to 2.6 times higher groundwater DSi concentration to support the BSi flux and keep the Lake 850 at steady-state. However, the BSi content is variable within the sedimentary basin, and thus the sedimentation rate is a crucial factor for the estimate of BSi accumulation. For future model improvement a monitoring of all inlets, groundwater, pore water, and the outlet together with sediment traps to constrain the production, BSi flux and dissolution would be needed.

8   Conclusions

The diatom-rich sediment in Lake 850 is formed because of high DSi supply by groundwater during the diatom growing season coupled with low sedimentation rates, which fosters a high accumulation of diatoms in the form of BSi. Water and Si mass balance demonstrated the importance of groundwater as a source of water and DSi, with fluxes that are 3 times greater than stream input. Groundwater supplies lighter δ^{30}Si, which is reflected in the lighter diatom δ^{30}Si ratio. By quantifying the groundwater inputs, the Si and Si isotopic mass balances allowed for the estimate of the stable Si isotope ratios of groundwater throughout the year. The modelled isotopic ratio of groundwater falls into the same range as the world groundwater δ^{30}Si ratio (Frings et al., 2016; Sutton et al., 2018).

Lakes on silica-rich bedrock, with low allochtonous input, low sedimentation rates, low-relief watershed geomorphology and high groundwater input have high potential to accumulate BSi. These water bodies with high BSi accumulation act as important sinks of Si in the global Si cycle. Our results support the importance of groundwater in the lake silicon budget and suggest that this process should not be overlooked in future investigations on BSi in lakes and global estimates of the terrestrial lake BSi sink.
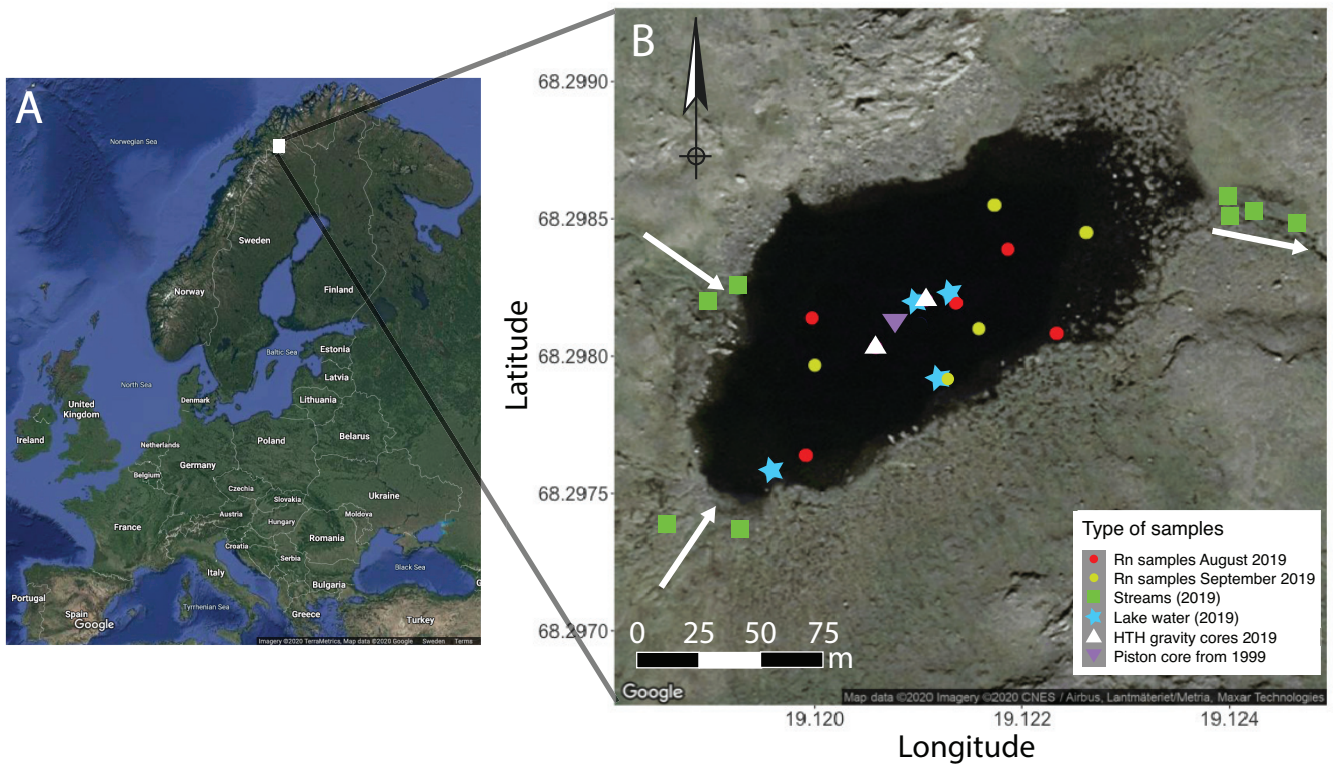
Figure 1. Sampling sites of Lake 850 (northern Sweden). Inlets and outlet streams are signified by white arrows. Plotted in R using package ggmaps (Kahle and Wickham, 2013) and modified.

Table 1. Summary of discharge from the inlets (Q_{in}), the outlet (Q_{out}) stream, groundwater discharge (Q_{gw}), dissolved Si concentration as $mg\,SiO_2\,l^{-1}$ in the inlets (c_{in}), the outlet (c_{out}), and the lake water (c_{lake}), stable Si isotopic signal of the inlet ($\delta^{30}Si_{in}$), outlet ($\delta^{30}Si_{out}$), and the lake ($\delta^{30}Si_{lake}$).

		March	June	July	August	September
Q_{in}	$l\,s^{-1}$		2.9	1.5	0.5	dry
Q_{out}	$l\,s^{-1}$		21.5	9.9	4.5	1.6
Q_{gw}	$l\,s^{-1}$	not sampled	not sampled	not sampled	3.58 ± 1.11	3.88 ± 0.86
c_{in}	$mg\,SiO_2\,l^{-1}$		2.34 ± 0.05	4.79 ± 0.05	5.05 ± 0.12	dry
c_{out}	$mg\,SiO_2\,l^{-1}$		1.19 ± 0.02	0.94 ± 0.01	1.12 ± 0.03	1.37 ± 0.01
c_{lake}	$mg\,SiO_2\,l^{-1}$	2.51 ± 0.35	1.24 ± 0.02	not sampled	0.96 ± 0.06	1.37 ± 0.04
$\delta^{30}Si_{in}$	‰		0.02 ± 0.10	0.72 ± 0.10	0.78 ± 0.15	dry
$\delta^{30}Si_{out}$	‰		0.89 ± 0.10	0.61 ± 0.10	0.79 ± 0.12	1.09 ± 0.20
$\delta^{30}Si_{lake}$	‰	1.27 ± 0.15	0.73 ± 0.10	not sampled	0.77 ± 0.32	1.02 ± 0.24
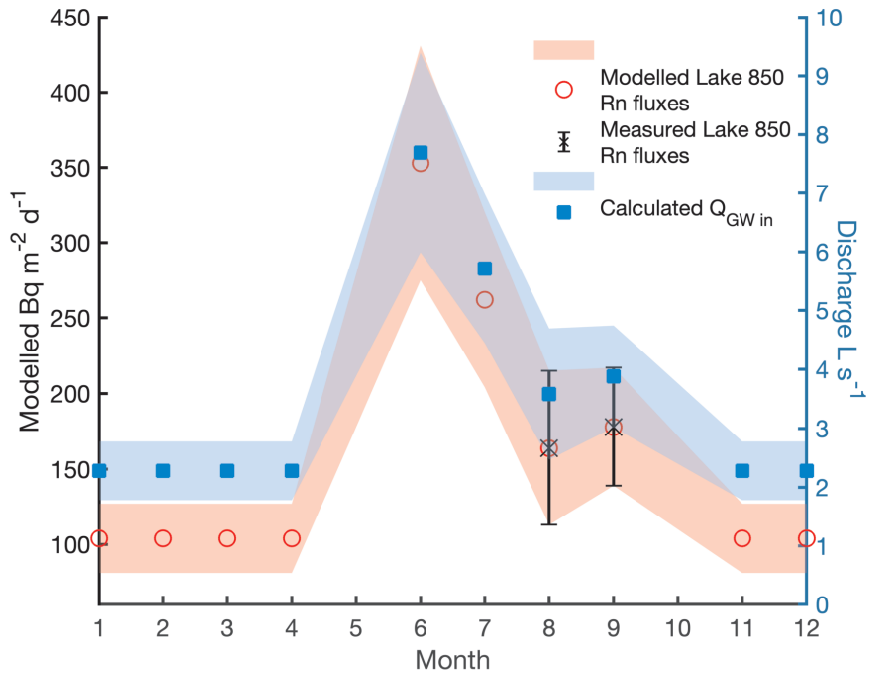
Figure 2. The modelled groundwater radon flux of Lake 850 (red circles) based on Rn fluxes in Lake Almberga in Abisko (*Olid et al., unpublished data*), the measured Rn fluxes in August and September (black cross), and the calculated groundwater discharge in $1s^{-1}$ throughout the year (blue squares). Uncertainties are shown as error bars and with shading.
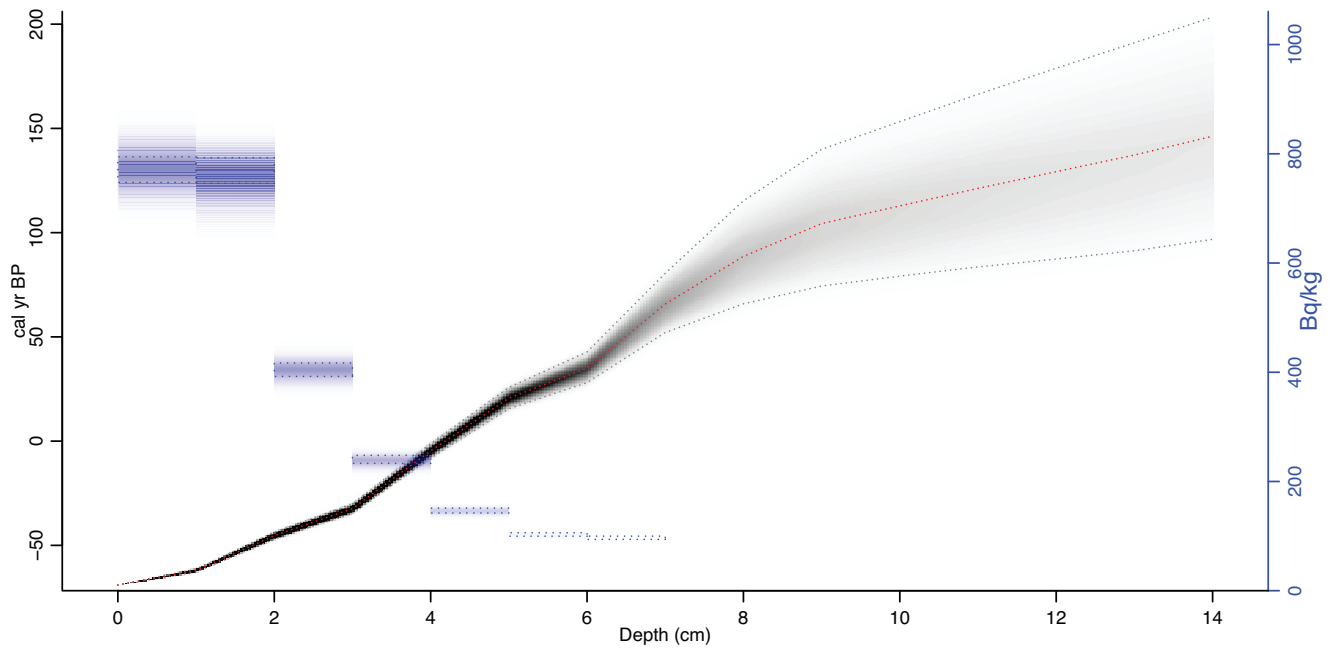
Figure 3. Age-depth model of the gravity core. Red line is the median probability age from all age-depth iterations. Grey shading represents age model probability and contains 95% confidence interval (dashed lines). The blue rectangles are the unsupported ^{210}Pb concentration in $\mathrm{Bq\,kg^{-1}}$.
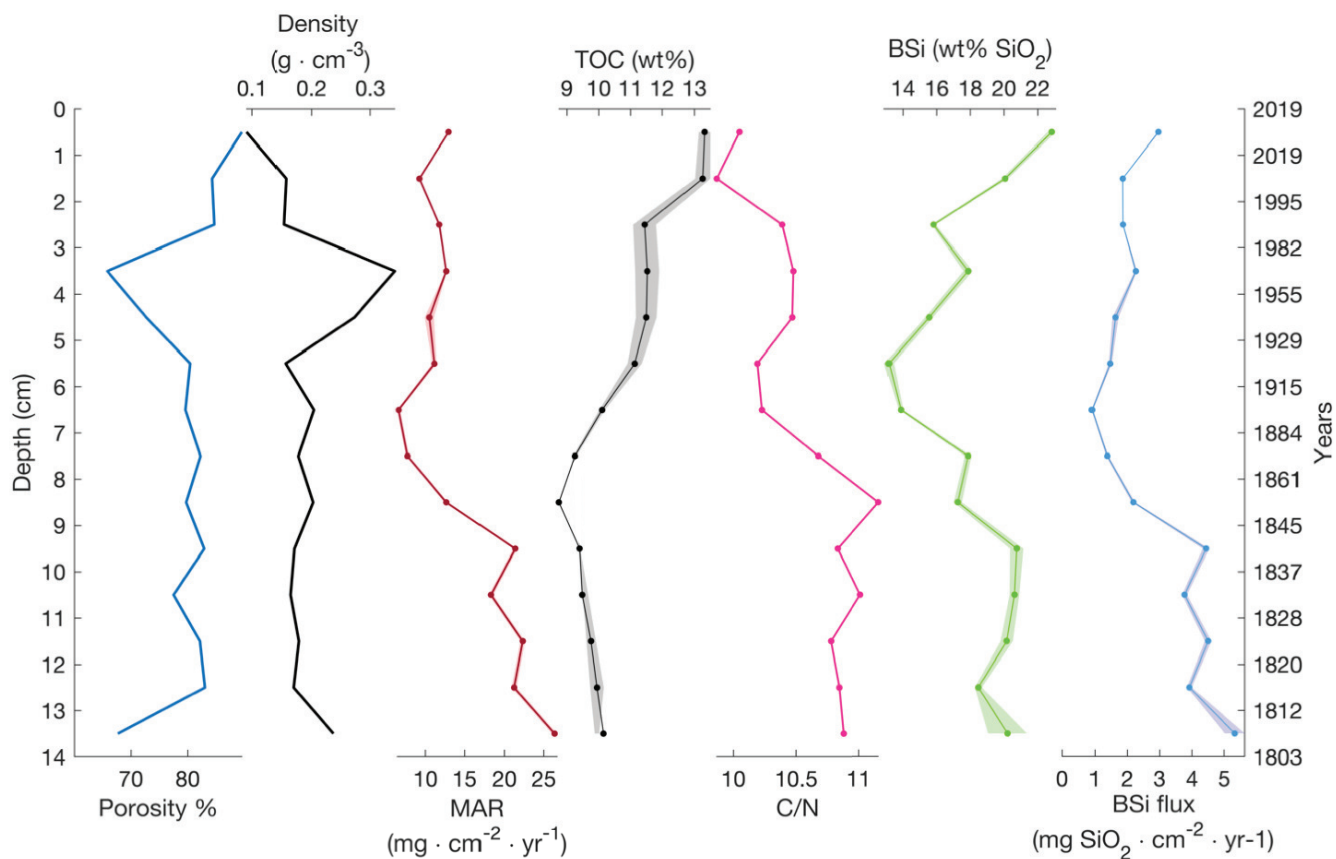
Figure 4. The gravity core sediment properties (porosity and dry bulk density), mass accumulation rate (MAR) and sediment density. Total organic carbon (TOC) and C/N showing changes in lake carbon content and sources. Biogenic silica (BSi) and BSi flux calculated from MAR and BSi concentrations. One standard deviation is shown by shading.
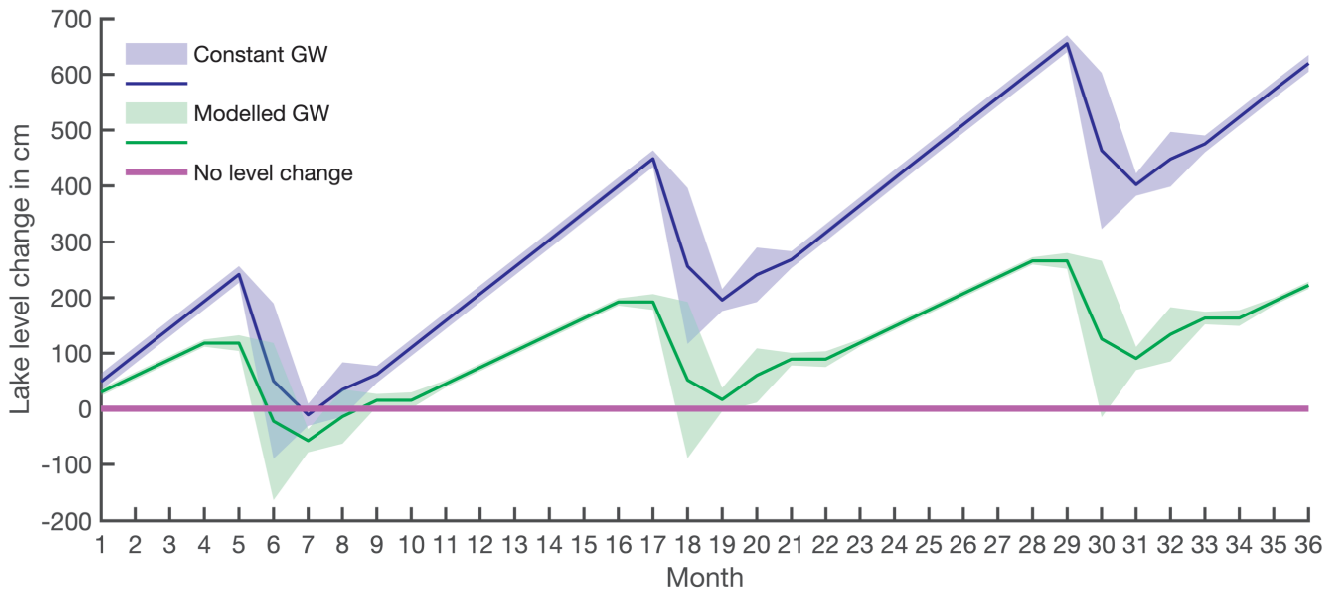
Figure 5. Long-term lake-level change calculated based on lake volume changes and water balance. The purple solid line indicates the lake-level starting point. The blue line with shading is the lake-level change with constant groundwater flow (scenario i), and the green line with shading is the lake-level change based on water balance with modelled groundwater discharges (scenario ii).
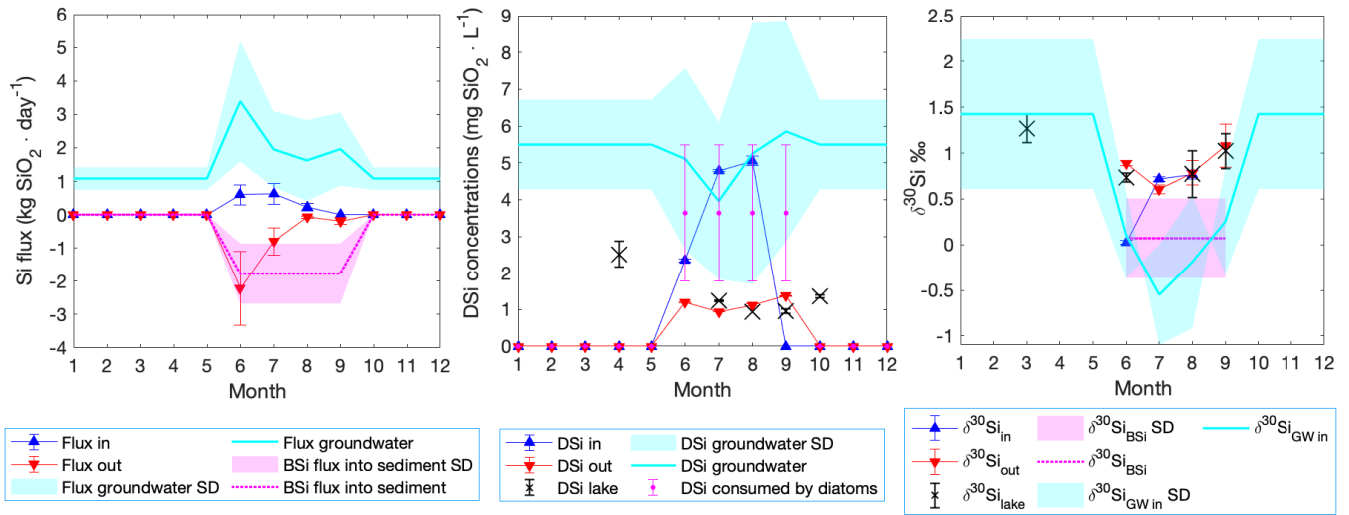
Figure 6. Si and Si isotope mass balance model of Lake 850 throughout the year. (A) Mass balance showing the stream DSi influx (blue triangles), the lake outlet DSi outflux as negative flux (red triangles), the diatom BSi flux based on a diatom bloom season lasting 4 months (magenta dotted line), also as a negative flux. The calculated groundwater DSi flux is shown as a positive flux (cyan line). (B) The monthly changes in the DSi concentration of the inlet (blue triangles), outlet (red triangles), lake (black crosses), diatom DSi uptake (magenta circles), and groundwater (cyan line). (C) The stable Si mass balance showing monthly variation of the isotopic composition of all DSi sources and sinks. Shading and error bars represent uncertainties.

Data availability. All data, if not directly available in tables and appendices, are available in the PANGAEA database. Alternatively all data are available upon request to the authors.

Author contributions. PZ and DJC designed the research. PZ and CO carried out the fieldwork. CO performed radon measurements and radon mass balance. PZ performed the TOC, TN, BSi, DSi, stable Si isotopes analyses and performed the data processing. All authors
505 contributed to discussion and data interpretation. PZ and CO wrote the paper with contributions and comments provided by JS, SCF, SO and DJC.

Competing interests. No competing interests are present.

Disclaimer. The authors declare that they have no conflict of interest.

Acknowledgements. This work was supported by The Royal Physiographic Society in Lund and by the Center for Geosphere Dynamics
510 (UNCE/SCI/006) to PZ, the Swedish Research Council to DJC, and NSF EAR-1514814 to SCF. Part of this work was supported by a FORMAS (d.nr. 2018-01217) grant attributed to CO. We also thank to Aldo Shemesh for providing diatom samples, Christian Bigler, Reiner Gielser and Carl-Magnus Mörth for advice and help with fieldwork design. Further we thank the organizations and the individuals who helped with the fieldwork and provided us with equipment and advice: Thomas Westin, Keith W. Larson, Erik Lundin, Svante Zachrisson, CIRC and field assistants Albin Bjärhall, Mathilde Schnuriger, Lukas Guth, Rosine Cartier, Geert Hensgens and Jan Foniok. We acknowledge
515 Hans Schöberg and Melanie Kielman for assistance during sample preparation and isotope data acquisition. This is Vegacenter contribution number #036.

References

ANS: Meteorological data from Abisko Observatory, daily mean 1913-01-01–2019-01-01, Abisko Scientific Research Station, 2020a.

ANS: Water discharge data from Miellejohka 685 m a.s.l., Abisko Scientific Research Station, 2020b.

Aquino-López, M. A., Blaauw, M., Christen, J. A., and Sanderson, N. K.: Bayesian Analysis of [210]Pb Dating, Journal of Agricultural, Biological and Environmental Statistics, 23, 317–333, https://doi.org/https://doi.org/10.1007/s13253-018-0328-7, 2018.

Barker, P. A., Hurrell, E. R., Leng, M. J., Plessen, B., Wolff, C., Conley, D. J., Keppens, E., Milne, I., Cumming, B. F., Laird, K. R., et al.: Carbon cycling within an East African lake revealed by the carbon isotope composition of diatom silica: a 25-ka record from Lake Challa, Mt. Kilimanjaro, Quaternary Science Reviews, 66, 55–63, https://doi.org/https://doi.org/10.1016/j.quascirev.2012.07.016, http://www.sciencedirect.com/science/article/pii/S0277379112002831, International Association of Limnogeology – Isotopes and Lakes, 2013.

Battarbee, R. W., Jones, V. J., Flower, R. J., Cameron, N. G., Bennion, H., Carvalho, L., and Juggins, S.: Diatoms, in: Tracking environmental change using lake sediments, edited by Smol, J. P., Birks, H. J. B., Last, W. M., Bradley, R. S., and Alverson, K., pp. 155–202, Springer, https://doi.org/10.1007/0-306-47668-1_8, 2002.

Bigler, C. and Hall, R. I.: Diatoms as indicators of climatic and limnological change in Swedish Lapland: a 100-lake calibration set and its validation for paleoecological reconstructions, Journal of Paleolimnology, 27, 97–115, https://doi.org/10.1023/A:1013562325326, https://doi.org/10.1023/A:1013562325326, 2002.

Brodie, C. R., Casford, J. S., Lloyd, J. M., Leng, M. J., Heaton, T. H., Kendrick, C. P., and Yongqiang, Z.: Evidence for bias in C/N, δ^{13}C and δ^{15}N values of bulk organic matter, and on environmental interpretation, from a lake sedimentary sequence by pre-analysis acid treatment methods, Quaternary Science Reviews, 30, 3076–3087, https://doi.org/10.1016/j.quascirev.2011.07.003, 2011.

Burnett, W. C. and Dulaiova, H.: Estimating the dynamics of groundwater input into the coastal zone via continuous radon-222 measurements, Journal of Environmental Radioactivity, 69, 21–35, https://doi.org/10.1016/s0265-931x(03)00084-5, 2003.

Campbell, D. H., Clow, D. W., Ingersoll, G. P., Mast, M. A., Spahr, N. E., and Turk, J. T.: Processes controlling the chemistry of two snowmelt-dominated streams in the Rocky Mountains, Water Resources Research, 31, 2811–2821, https://doi.org/10.1029/95wr02037, 1995.

Chanyotha, S., Kranrod, C., and Burnett, W. C.: Assessing diffusive fluxes and pore water radon activities via a single automated experiment, Journal of Radioanalytical and Nuclear Chemistry, 301, 581–588, https://doi.org/10.1007/s10967-014-3157-3, 2014.

Clarke, J.: The occurrence and significance of biogenic opal in the regolith, Earth-Science Reviews, 60, 175–194, https://doi.org/10.1016/s0012-8252(02)00092-2, 2003.

Clow, D., Schrott, L., Webb, R., Campbell, D., Torizzo, A., and Dornblaser, M.: Ground water occurrence and contributions to streamflow in an alpine catchment, Colorado Front Range, Groundwater, 41, 937–950, https://doi.org/10.1111/j.1745-6584.2003.tb02436.x, 2003.

Conger, P. S.: Accumulation of diatomaceous deposits, Journal of Sedimentary Research, 12, 55–66, https://doi.org/10.1306/d4269143-2b26-11d7-8648000102c1865d, 1942.

Conley, D. J.: Biogenic silica as an estimate of siliceous microfossil abundance in Great Lakes sediments, Biogeochemistry, 6, 161–179, https://doi.org/10.1007/bf02182994, 1988.

Conley, D. J.: An interlaboratory comparison for the measurement of biogenic silica in sediments, Marine Chemistry, 63, 39–48, https://doi.org/10.1016/s0304-4203(98)00049-8, 1998.

Conley, J. D. and Schelske, C.: Biogenic Silica, vol. 1, pp. 281–293, Springer Netherlands, Dordrecht, https://doi.org/10.1007/0-306-47668-1_14, 2001.

555 De La Rocha, C. L., Brzezinski, M. A., and Deniro, M. J.: Fractionation of silicon isotopes by marine diatoms during biogenic silica formation, Geochimica et Cosmochimica Acta, 61, 5051–5056, https://doi.org/10.1016/s0016-7037(97)00300-1, 1997.

Dimova, N. T. and Burnett, W. C.: Evaluation of groundwater discharge into small lakes based on the temporal distribution of radon-222, Limnology and Oceanography, 56, 486–494, https://doi.org/10.4319/lo.2011.56.2.0486, 2011.

Dimova, N. T., Burnett, W. C., Chanton, J. P., and Corbett, J. E.: Application of radon-222 to investigate groundwater discharge into small

560 shallow lakes, Journal of Hydrology, 486, 112–122, https://doi.org/10.1016/j.jhydrol.2013.01.043, 2013.

Fortin, M.-C. and Gajewski, K.: Assessing the use of sediment organic, carbonate and biogenic silica content as indicators of environmental conditions in Arctic lakes, Polar Biology, 32, 985–998, https://doi.org/10.1007/s00300-009-0598-1, 2009.

Frings, P. J., Clymans, W., Jeppesen, E., Lauridsen, T. L., Struyf, E., and Conley, D. J.: Lack of steady-state in the global biogeochemical Si cycle: emerging evidence from lake Si sequestration, Biogeochemistry, 117, 255–277, https://doi.org/10.1007/s10533-013-9944-z,

565 https://doi.org/10.1007/s10533-013-9944-z, 2014.

Frings, P. J., Claymans, W., Fontorbe, G., Rocha, C. L. D. L., and Conley, D. J.: The continental Si cycle and its impact on the ocean Si isotope budget, Chemical Geology, 425, 12–36, https://doi.org/10.1016/j.chemgeo.2016.01.020, 2016.

Georg, R., Reynolds, B., Frank, M., and Halliday, A.: New sample preparation techniques for the determination of Si isotopic compositions using MC-ICPMS, Chemical Geology, 235, 95 – 104, https://doi.org/http://dx.doi.org/10.1016/j.chemgeo.2006.06.006, http:

570 //www.sciencedirect.com/science/article/pii/S000925410600307X, 2006.

Georg, R., West, A., Basu, A., and Halliday, A.: Silicon fluxes and isotope composition of direct groundwater discharge into the Bay of Bengal and the effect on the global ocean silicon isotope budget, Earth and Planetary Science Letters, 283, 67–74, https://doi.org/10.1016/j.epsl.2009.03.041, 2009.

Hood, J. L., Roy, J. W., and Hayashi, M.: Importance of groundwater in the water balance of an alpine headwater lake, Geophysical Research

575 Letters, 33, https://doi.org/10.1029/2006gl026611, 2006.

Hurley, J. P., Armstrong, D. E., Kenoyer, G. J., and Bowser, C. J.: Ground water as a silica source for diatom production in a precipitation-dominated lake, Science, 227, 1576–1578, https://doi.org/10.1126/science.227.4694.1576, 1985.

Huth, A., Leydecker, A., Sickman, J., and Bales, R.: A two-component hydrograph separation for three high-elevation catchments in the Sierra Nevada, California, Hydrological Processes, 18, 1721–1733, https://doi.org/10.1002/hyp.1414, 2004.

580 Jenny, H.: Factors of Soil Formation: A System of quantitative Pedology, New York: McGraw-Hill., 1941.

Johnson, T. C., Brown, E. T., and Shi, J.: Biogenic silica deposition in Lake Malawi, East Africa over the past 150,000 years, Palaeogeography, Palaeoclimatology, Palaeoecology, 303, 103–109, https://doi.org/10.1016/j.palaeo.2010.01.024, 2011.

Kahle, D. and Wickham, H.: ggmap: Spatial Visualization with ggplot2, The R Journal, 5, 144–161, https://doi.org/10.32614/rj-2013-014, https://journal.r-project.org/archive/2013-1/kahle-wickham.pdf, 2013.

585 Kaplan, M. R., Wolfe, A. P., and Miller, G. H.: Holocene environmental variability in southern Greenland inferred from lake sediments, Quaternary Research, 58, 149–159, https://doi.org/10.1006/qres.2002.2352, 2002.

Kenoyer, G. J. and Anderson, M. P.: Groundwater's dynamic role in regulating acidity and chemistry in a precipitation-dominated lake, Journal of Hydrology, 109, 287–306, 1989.

Leng, M. J., Swann, G. E., Hodson, M. J., Tyler, J. J., Patwardhan, S. V., and Sloane, H. J.: The potential use of silicon isotope composition

590 of biogenic silica as a proxy for environmental change, Silicon, 1, 65–77, https://doi.org/10.1007/s12633-009-9014-2, 2009.

Liu, F., Williams, M. W., and Caine, N.: Source waters and flow paths in an alpine catchment, Colorado Front Range, United States, Water Resources Research, 40, https://doi.org/10.1029/2004wr003076, 2004.

Maavara, T., Slowinski, S., Rezanezhad, F., Van Meter, K., and Van Cappellen, P.: The role of groundwater discharge fluxes on Si: P ratios in a major tributary to Lake Erie, Science of the Total Environment, 622, 814–824, https://doi.org/10.1016/j.scitotenv.2017.12.024, 2018.

595 MacIntyre, S., Wanninkhof, R., and Chanton, J.: Trace gas exchange across the air-water interface in freshwater and coastal marine environments, pp. 52–97, Blackwell Science Ltd, 1995.

McKay, N. P., Kaufman, D. S., and Michelutti, N.: Biogenic silica concentration as a high-resolution, quantitative temperature proxy at Hallet Lake, south-central Alaska, Geophysical Research Letters, 35, https://doi.org/10.1029/2007gl032876, 2008.

Newberry, T. L. and Schelske, C. L.: Biogenic silica record in the sediments of Little Round Lake, Ontario, Hydrobiologia, 143, 293–300,
600 https://doi.org/10.1007/978-94-009-4047-5_37, 1986.

NORM, I.: Guide to expression of uncertainty in measurement. Corrected and Reprinted, International Organization for Standardization, Geneva, Switzerland, 1995.

Opfergelt, S. and Delmelle, P.: Silicon isotopes and continental weathering processes: Assessing controls on Si transfer to the ocen, Comptes Rendus Geoscience, 344, 723–738, https://doi.org/10.1016/j.crte.2012.09.006, 2012.

605 Opfergelt, S., Eiriksdottir, E. S., Burton, K. W., Einarsson, A., Siebert, C., Gislason, S. R., and Halliday, A. N.: Quantifying the impact of freshwater diatom productivity on silicon isotopes and silicon fl uxes: Lake Myvatn, Iceland, Earth and Planetary Science Letters, 305, 73–82, https://doi.org/10.1016/j.epsl.2011.02.043, http://dx.doi.org/10.1016/j.epsl.2011.02.043, 2011.

Pienitz, R., Doran, P., and Lamoureux, S.: Origin and geomorphology of lakes in the polar regions, Oxford University Press, https://doi.org/10.1093/acprof:oso/9780199213887.003.0002, https://oxford.universitypressscholarship.com/view/10.1093/acprof:
610 oso/9780199213887.001.0001/acprof-9780199213887-chapter-2, 2008.

Plunkett, G. M., Whitehouse, N. J., Hall, V. A., Brown, D. M., and Baillie, M. G. L.: A precisely-dated lake-level rise marked by diatomite formation in northeastern Ireland, Journal of Quaternary Science, 19, 3–7, https://doi.org/10.1002/jqs.816, https://onlinelibrary.wiley.com/doi/abs/10.1002/jqs.816, 2004.

Pokrovsky, O., Reynolds, B., Prokushkin, A., Schott, J., and Viers, J.: Silicon isotope variations in Central Siberian rivers during basalt weath-
615 ering in permafrost-dominated larch forests, Chemical Geology, 355, 103–116, https://doi.org/10.1016/j.chemgeo.2013.07.016, 2013.

Reynolds, B. C., Aggarwal, J., Andre, L., Baxter, D., Beucher, C., Brzezinski, M. A., Engstrom, E., Georg, R. B., Land, M., Leng, M. J., Opfergelt, S., Rodushkin, I., Sloane, H. J., van den Boorn, S. H. J. M., Vroon, P. Z., and Cardinal, D.: An inter-laboratory comparison of Si isotope reference materials, Journal of Analytical Atomic Spectrometry, 22, 561–568, https://doi.org/10.1039/b616755a, http://dx.doi.org/10.1039/B616755A, 2007.

620 Rosén, P., Vogel, H., Cunningham, L., Reuss, N., Conley, D. J., and Persson, P.: Fourier transform infrared spectroscopy, a new method for rapid determination of total organic and inorganic carbon and biogenic silica concentration in lake sediments, Journal of Paleolimnology, 43, 247–259, https://doi.org/10.1007/s10933-009-9329-4, 2010.

Rubensdotter, L. and Rosqvist, G.: The effect of geomorphological setting on Holocene lake sediment variability, northern Swedish Lapland, Journal of Quaternary Science, 18, 757–767, https://doi.org/10.1002/jqs.800, 2003.

625 Russell, J. M. and Johnson, T. C.: A high-resolution geochemical record from Lake Edward, Uganda Congo and the timing and causes of tropical African drought during the late Holocene, Quaternary Science Reviews, 24, 1375–1389, https://doi.org/10.1016/j.quascirev.2004.10.003, 2005.

Ryves, D. B., Jewson, D. H., Sturm, M., Battarbee, R. W., Flower, R. J., Mackay, A. W., and Granin, N. G.: Quantitative and qualitative relationships between planktonic diatom communities and diatom assemblages in sedimenting material and surface sediments in Lake Baikal, Siberia, Limnology and Oceanography, 48, 1643–1661, https://doi.org/10.4319/lo.2003.48.4.1643, 2003.

Schelske, C. L.: Biogeochemical silica mass balances in Lake Michigan and Lake Superior, Biogeochemistry, 1, 197–218, https://doi.org/10.1007/bf02187199, 1985.

Schubert, M., Paschke, A., Lieberman, E., and Burnett, W. C.: Air–water partitioning of ^{222}Rn and its dependence on water temperature and salinity, Environmental Science & Technology, 46, 3905–3911, https://doi.org/10.1021/es204680n, 2012.

Shemesh, A., Rosqvist, G., Rietti-Shati, M., Rubensdotter, L., Bigler, C., Yam, R., and Karlén, W.: Holocene climatic change in Swedish Lapland inferred from an oxygen-isotope record of lacustrine biogenic silica, The Holocene, 11, 447–454, 2001.

Strickland, J. and Parsons, T.: A practical handbook of seawater analysis, second edition edn., 1972.

Struyf, E., Mörth, C.-M., Humborg, C., and Conley, D. J.: An enormous amorphous silica stock in boreal wetlands, Journal of Geophysical Research: Biogeosciences, 115, https://doi.org/10.1029/2010jg001324, 2010.

Sun, X., Andersson, P., Land, M., Humborg, C., and Mörth, C.-M.: Stable silicon isotope analysis on nanomole quantities using MC-ICP-MS with a hexapole gas-collision cell, Journal of Analytical Atomic Spectrometry, 25, 156–162, 2010.

Sutton, J. N., André, L., Cardinal, D., Conley, D. J., De Souza, G. F., Dean, J., Dodd, J., Ehlert, C., Ellwood, M. J., Frings, P. J., et al.: A review of the stable isotope bio-geochemistry of the global silicon cycle and its associated trace elements, Frontiers in Earth Science, 5, 112, https://doi.org/10.3389/feart.2017.00112, 2018.

Swann, G. E. and Mackay, A. W.: Potential limitations of biogenic silica as an indicator of abrupt climate change in Lake Baikal, Russia, Journal of Paleolimnology, 36, 81–89, https://doi.org/10.1007/s10933-006-0005-7, 2006.

Tallberg, P., Opfergelt, S., Cornelis, J.-T., Liljendahl, A., and Weckström, J.: High concentrations of amorphous, biogenic Si (BSi) in the sediment of a small high-latitude lake: implications for biogeochemical Si cycling and for the use of BSi as a paleoproxy, Aquatic Sciences, 77, 293–305, https://doi.org/10.1007/s00027-014-0387-y, 2015.

Taylor, B. N. and Kuyatt, C. E.: Guidelines for evaluating and expressing the uncertainty of NIST measurement results, https://doi.org/10.6028/nist.tn.1297-1993, 1994.

Theriot, E. C., Fritz, S. C., Whitlock, C., and Conley, D. J.: Late Quaternary rapid morphological evolution of an endemic diatom in Yellowstone Lake, Wyomin, Paleobiology, 32, 38–54, https://doi.org/10.1666/02075.1, 2006.

Treguer, P., Nelson, D. M., Van Bennekom, A. J., DeMaster, D. J., Leynaert, A., and Queguiner, B.: The silica balance in the world ocean: a reestimate, Science, 268, 375–379, https://doi.org/10.1126/science.268.5209.375, 1995.

Tréguer, P. J. and De La Rocha, C. L.: The world ocean silica cycle, Annual Review of Marine Science, 5, 477–501, 2013.

Turnipseed, D. and Sauer, V.: Discharge measurements at gaging stations: US Geological Survey Techniques and Methods, book 3, chap, 2010.

Vachon, D. and Prairie, Y. T.: The ecosystem size and shape dependence of gas transfer velocity versus wind speed relationships in lakes, Canadian Journal of Fisheries and Aquatic Sciences, 70, 1757–1764, https://doi.org/10.1139/cjfas-2013-0241, 2013.

Varela, D. E., Pride, C. J., and Brzezinski, M. A.: Biological fractionation of silicon isotopes in Southern Ocean surface waters, Global Biogeochemical Cycles, 18, https://doi.org/10.1029/2003gb002140, 2004.

Wolfe, A. P., Miller, G. H., Olsen, C. A., Forman, S. L., Doran, P. T., and Holmgren, S. U.: Geochronology of high latitude lake sediments, in: Long-term environmental change in Arctic and Antarctic lakes, pp. 19–52, Springer, 2004.

665   Zhang, A., Zhang, J., and Liu, S.: Spatial and temporal variations of dissolved silicon isotope compositions in a large dammed river system, Chemical Geology, p. 119645, https://doi.org/10.1016/j.chemgeo.2020.119645, 2020.

Ziegler, K., Chadwick, O. A., Brzezinski, M. A., and Kelly, E. F.: Natural variations of δ^{30}Si ratios during progressive basalt weathering, Hawaiian Islands, Geochimica et Cosmochimica Acta, 69, 4597–4610, https://doi.org/10.1016/j.gca.2005.05.008, 2005.

Appendix A: Methods

A1 Modelling groundwater Rn fluxes

Radon fluxes from Lake Almberga from the Abisko region were estimated using the same approach in summer and autumn 2018 and 2019 (*C.Olid, unpublished data*). The derived Rn fluxes obtained from the lake survey were used here to model groundwater fluxes through the year in Lake 850. To do this, we divided the estimated groundwater Rn flux from the Rn mass balance in Lake 850 in September ($178 \pm 39 \, \mathrm{Bq\,m^{-2}\,d^{-1}}$) by the mean groundwater Rn flux obtained from the lake survey in September ($104 \pm 10 \, \mathrm{Bq\,m^{-2}\,d^{-1}}$, *C. Olid, unpublished data*). The derived ratio (1.71) was then multiplied by the mean groundwater Rn fluxes from the lake survey to model the groundwater Rn fluxes in Lake 850 for those months were Rn measurements were not available (June, July and September). Rn fluxes through groundwater during the ice-covered period were assumed to be 59% of September fluxes (*C. Olid, unpublished data*; Figure 2; Table A1). The groundwater Rn flux from November to April was assumed to be constant and equal to April estimations.

A2 Groundwater DSi and $\delta^{30}Si$ calculations during the ice-covered period

The groundwater concentration c_{gw} in during the ice-covered period was calculated from the groundwater discharge, the lake volume from the water balance, and the lake DSi differences between September and March though a mixing model:

$$c_{\mathrm{gw}} = \frac{(c_{\mathrm{Mar}} \cdot (V_{\mathrm{Sept}} + V_{\mathrm{gw}})) - (c_{\mathrm{Sept}} \cdot V_{\mathrm{Sept}})}{V_{\mathrm{gw}}} \tag{A1}$$

where c_{Mar} is the lake concentration in March, c_{Sept} is the lake concentration in September, V_{Sept} is the lake volume in September, and V_{gw} in is the total volume of water brought by groundwater in 8 months. The total water volume brought by groundwater in 8 months was calculated from the modelled groundwater winter discharges (Figure 2). The lake volume in September is taken from the water balance model, where the modelled groundwater discharges were used (Figure 5 and A1, green line).

Similarly, the c_{gw} in during the ice-covered period in the scenario with continuous BSi flux to the sediment for period of 8 month was calculated by adding flux into the sediment into the mixing model:

$$c_{\mathrm{gw}} = \frac{(c_{\mathrm{Mar}} \cdot (V_{\mathrm{Sept}} + V_{\mathrm{gw}})) - (c_{\mathrm{Sept}} \cdot V_{\mathrm{Sept}}) + \phi_{\mathrm{BSi}}}{V_{\mathrm{gw}}} \tag{A2}$$

where the ϕ_{BSi} is the total flux of BSi to sediment in 8 months. The BSi flux into the sediment for 8 months was calculated as a sum of the continuous monthly BSi flux from September until March.

Table A1. Estimated Rn fluxes in August and September with the derived water discharges through groundwater based on the Rn mass balance.

Measure data	$\mathrm{Bq\,m^{-2}\,d^{-1}}$	SD	Month	$\frac{\mathrm{Rn_{L850}}}{\mathrm{Rn_{Almberga}}}$	$Q\,[\mathrm{m^3\,d^{-1}}]$	SD
08/2019	164	51	8		309	108
09/2019	178	39	9	1.71	335	92
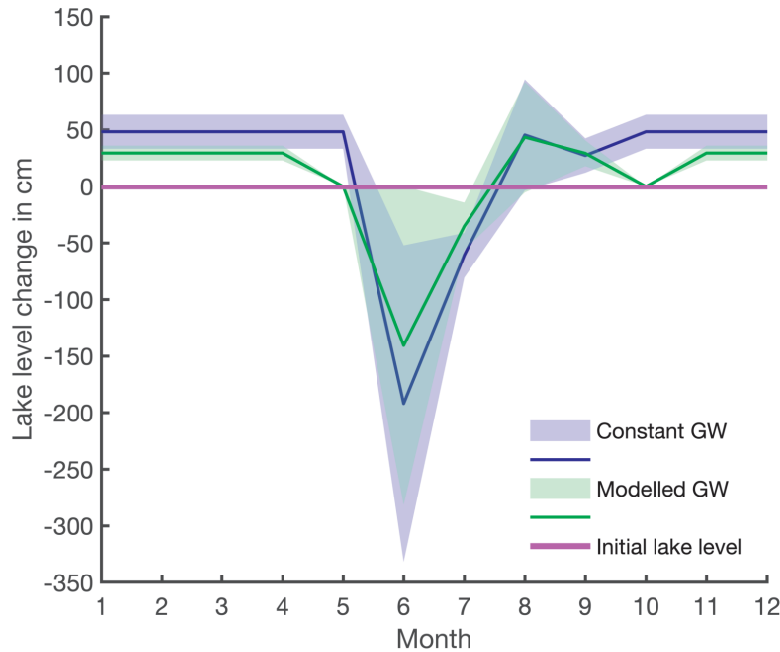
Figure A1. Estimated lake-level variation between neighbouring months throughout the year with uncertainties as shading. No lake-level change is depicted by the solid purple line. The blue line presents lake-level increase or decrease from one to another month with constant groundwater discharge (scenario i), and the green line is the rate of lake-level variation with modelled groundwater discharges (scenario ii).

The isotopic composition of the groundwater during the ice-covered period, based on measured data was calculated as:

$$\delta^{30}\mathrm{Si}_{\mathrm{gw}} = \frac{\delta^{30}\mathrm{Si}_{\mathrm{Mar}} \cdot ((c_{\mathrm{Sept}} \cdot V_{\mathrm{Sept}}) + (c_{\mathrm{gw}} \cdot V_{\mathrm{gw}})) - \delta^{30}\mathrm{Si}_{\mathrm{Sept}} \cdot (c_{\mathrm{Sept}} \cdot V_{\mathrm{Sept}})}{c_{\mathrm{gw}} \cdot V_{\mathrm{gw}}} \tag{A3}$$

where $\delta^{30}\mathrm{Si}_{\mathrm{Mar}}$ is the lake isotopic composition in March, $\delta^{30}\mathrm{Si}_{\mathrm{Sept}}$ is the lake isotopic composition in September, c_{Sept} is the lake concentration in September, c_{gw} in is the concentration of groundwater during the ice-covered period (eq. A1 or A2, depending on model), V_{gw} in is the total volume of water brought by groundwater in 8 months, and V_{Sept} is the lake volume in September.

A3   Silicon isotope mass balance – $\delta^{30}Si_{gw}$ calculation

Due to the high groundwater input in Lake 850 proven by the Rn mass balance (see section Results: 5.2 Groundwater discharge), the inlet δ^{30}Si does not represent the initial δ^{30}Si used by diatoms. Therefore, the initial δ^{30}Si of DSi is a mixture of groundwater δ^{30}Si and inlet δ^{30}Si flux weighted. The $\delta^{30}\mathrm{Si}_{\mathrm{initial}}$ in was calculated from $\delta^{30}\mathrm{Si}_{\mathrm{postuptake}}$, which equals to $\delta^{30}\mathrm{Si}_{\mathrm{lake}}$ as:

$$\delta^{30}\mathrm{Si}_{\mathrm{initial}} = \delta^{30}\mathrm{Si}_{\mathrm{postuptake}} + {}^{30}\varepsilon \cdot \left(1 - \frac{c_{\mathrm{out}}}{c_{\mathrm{initial}}}\right) \tag{A4}$$

Table B1. A summary of all 3 scenarios, which were examined through Si and Si isotope mass balance models

scenario	BSi flux time	daily BSi flux	range c_{gw}	range $\delta^{30}Si_{gw}$	DSi% consumed by production	range $\delta^{30}Si_{BSi}$
1	12 months	$0.58\,\mathrm{kg\,SiO_2\,day^{-1}}$	1.40 to 8.46 $\mathrm{mg\,SiO_2\,l^{-1}}$	-0.64 to $1.37‰$	$39-61\%$	-0.49 to $-0.01‰$
2	4 month	$1.77\,\mathrm{kg\,SiO_2\,day^{-1}}$	3.96 to 5.85 $\mathrm{mg\,SiO_2\,l^{-1}}$	-0.55 to $1.43‰$	$73-79\%$	-0.49 to $-0.01‰$
3	1 month	$7.08\,\mathrm{kg\,SiO_2\,day^{-1}}$	0.37 to 13.10 $\mathrm{mg\,SiO_2\,l^{-1}}$	-0.09 to $1.43‰$	$0-88\%$	$-0.21‰$

Further the groundwater $\delta^{30}Si_{gw}$ which fits the measured data and keeps the steady-state, was calculated as:

$$\delta^{30}Si_{gw} = \frac{\delta^{30}Si_{initial} \cdot ((c_{in} \cdot Q_{in}) + (c_{gw} \cdot Q_{gw})) - \delta^{30}Si_{in} \cdot (c_{in} \cdot Q_{in})}{c_{gw} \cdot Q_{gw}} \tag{A5}$$

Appendix B: Mass balance models: Extreme Si and Si isotope mass balances

The Si and Si isotopic mass balances models were tested for two extreme scenarios to model the highest and the lowest possible concentration of groundwater brought into the lake. Further, a scenario based on recent diatom growth season is modelled (Table B1). The DSi concentration and isotopic composition from the inlet and outlet streams are similar in all three scenarios. The groundwater DSi concentrations and isotopic composition are calculated from the groundwater fluxes influenced by the three potential BSi fluxes into the sediment, representing three possible lengths of diatom production. All scenarios are using the open system isotopic model (Varela et al., 2004) to describe the effect of diatom production on the lake water $\delta^{30}Si$ ratio. The difference between the first and second scenario is the BSi flux into the sediment: (1) considers BSi flux into the sediment throughout the whole year representing lack of ice-covered period, and (2) BSi flux into sediment is present only from June until September (Shemesh et al., 2001). Scenario (3) utilizes the open system isotopic model only for June, with no diatom production the rest of the year, and thus no fractionation in the lake, which describes lake behaviour with only short ice-free period. Here we describe only scenario 1 and 3, whereas in the main text scenario 2 is presented and discussed.

B1   Scenario 1: 12 months of BSi flux into sediment

A scenario assuming a constant BSi flux to the sediment throughout the year (magenta line, Figure B1A) simulates a situation when climate is warming, and the diatom growth season is prolonged to maximum. Additionally, this scenario was characterized by the minimal groundwater fluxes and DSi concentrations. The DSi removal by diatoms is of $1.21 \pm 0.62\,\mathrm{mg\,SiO_2\,l^{-1}}$ SiO_2 monthly (magenta points, Figure B1B). Therefore, with an added BSi flux of $0.58 \pm 0.29\,\mathrm{kg}$ SiO_2 per day, the lake inlet does not supply sufficient DSi for diatoms to grow. The groundwater DSi concentration is calculated as the DSi flux needed to keep the lake balanced and sustain the diatom production. The groundwater flux of DSi varies from 0.43 ± 0.51 to $2.20 \pm 1.37\,\mathrm{kg}$ SiO_2 per day, depending on the season (cyan line, Figure B1A). The highest groundwater DSi flux occurs in June, followed

by a decreasing trend towards August, when it reaches the minimum. From August until November, the groundwater DSi flux increases and is stabilized after November, and it is constant until May. From the calculated groundwater flux, the groundwater concentration is between $1.40 \pm 1.59 \, \mathrm{mg\,SiO_2\,l^{-1}}$ to $3.32 \pm 1.93 \, \mathrm{mg\,SiO_2\,l^{-1}}$ during the ice-free period, and, when combined with the lake DSi deficiency at the end of the season, it is $8.46 \pm 0.40 \, \mathrm{mg\,SiO_2\,l^{-1}}$ (cyan line, Figure B1B) in the ice-covered period.

In scenario 1, with constant BSi flux into the sediment during the whole year of $0.58 \pm 0.29 \, \mathrm{kg\,SiO_2}$ per day, high superficial and groundwater discharges occur in June, with DSi concentrations of 2.34 and $3.32 \, \mathrm{mg\,SiO_2\,l^{-1}}$, respectively (Figure B1B). The stream inlet has a light isotopic ratio of $\delta^{30}\mathrm{Si_{in}} = 0.02 \pm 0.10\text{‰}$. The initial DSi available for diatoms is a mixture of the groundwater and the stream inlet, with $\delta^{30}\mathrm{Si_{inital}} = 0.22 \pm 0.36\text{‰}$. The groundwater was calculated from the $\delta^{30}\mathrm{Si_{inital}}$ to have an isotopic ratio of $\delta^{30}\mathrm{Si_{gw}} = 0.27 \pm 0.51\text{‰}$ in June. Thus, the expected BSi isotopic ratio was calculated to be $-0.21 \pm 0.42\text{‰}$, which is within the range of mean measured $\delta^{30}\mathrm{Si_{BSi}} = 0.07 \pm 0.43\text{‰}$ in the top sediment layers. The diatom production consumes approximately 61% of the DSi influx in June.

Although groundwater discharge culminates in July, compared with the decreasing trend in the stream inlet, the isotopic composition of the lake in July is influenced by both the groundwater and the stream. The DSi concentration of the inlet is $4.79 \pm 0.03 \, \mathrm{mg\,SiO_2\,l^{-1}}$, but with 4 times lower discharge than groundwater. The calculated groundwater DSi concentration from the steady-state model is only $1.56 \pm 0.95 \, \mathrm{mg\,SiO_2\,l^{-1}}$ (Figure B1B). Further, the initial isotopic mixture for diatom growth $\delta^{30}\mathrm{Si_{initial}} = -0.03 \pm 0.10\text{‰}$ is composed of the stream $\delta^{30}\mathrm{Si_{in}} = 0.72 \pm 0.10\text{‰}$ and the groundwater $\delta^{30}\mathrm{Si_{gw}} = -0.64 \pm 0.46\text{‰}$ (Figure B1C). The expected BSi isotopic ratio is $\delta^{30}\mathrm{Si_{BSi}} = -0.49 \pm 0.21\text{‰}$, which still falls within the mean measured $\delta^{30}\mathrm{Si_{BSi}} = 0.07 \pm 0.43\text{‰}$ in the sediment. The diatom production in July consumes 58% of the DSi.

In August, the isotopic composition of the stream inlet, lake, and outlet are similar. The DSi concentration of the inlet is at its maximum, with an isotopic composition of $0.78 \pm 0.15\text{‰}$, but due to a very low inlet discharge it is not affecting the lake. The concentration and isotopic ratio of the outlet and the lake are almost identical, thus, the groundwater input is $1.40 \pm 1.59 \, \mathrm{mg\,SiO_2\,l^{-1}}$ of DSi (Figure B1B), with an isotopic ratio of $\delta^{30}\mathrm{Si_{gw}} = 0.14 \pm 0.73\text{‰}$ (Figure B1C). The expected BSi isotopic ratio is $\delta^{30}\mathrm{Si_{BSi}} = -0.31 \pm 0.67\text{‰}$, which is in agreement with the mean measured $\delta^{30}\mathrm{Si_{BSi}}$ in the diatoms from sediment. The diatom production in August consumes 39% of the lake DSi.

September is the last month before the lake is ice-covered. There is no stream inlet, as the watershed is snow-covered. The groundwater input, with a concentration of $2.31 \pm 1.03 \, \mathrm{mg\,SiO_2\,l^{-1}}$, is four times higher than the removal by the lake outlet. This suggests that the lake-level is changing throughout seasons, which is not considered in any of the Si mass balance and isotopic models examined. The lake DSi of $1.37 \pm 0.04 \, \mathrm{mg\,SiO_2\,l^{-1}}$ is fully influenced by groundwater and diatom production. The groundwater isotopic ratio is $0.65 \pm 0.55\text{‰}$, and the diatom production is using 41% of the lake DSi. The expected BSi isotopic ratio is $\delta^{30}\mathrm{Si_{BSi}} = -0.01 \pm 0.47\text{‰}$, which is in agreement with the mean measured $\delta^{30}\mathrm{Si_{BSi}}$ in the diatoms from sediment.

This scenario assumes that the groundwater concentration during the ice-covered lake is recharging the lake DSi, while the BSi flux into the sediment is still present (Figure B1B). Applying the mixing model (equation A2 and A3), groundwater DSi
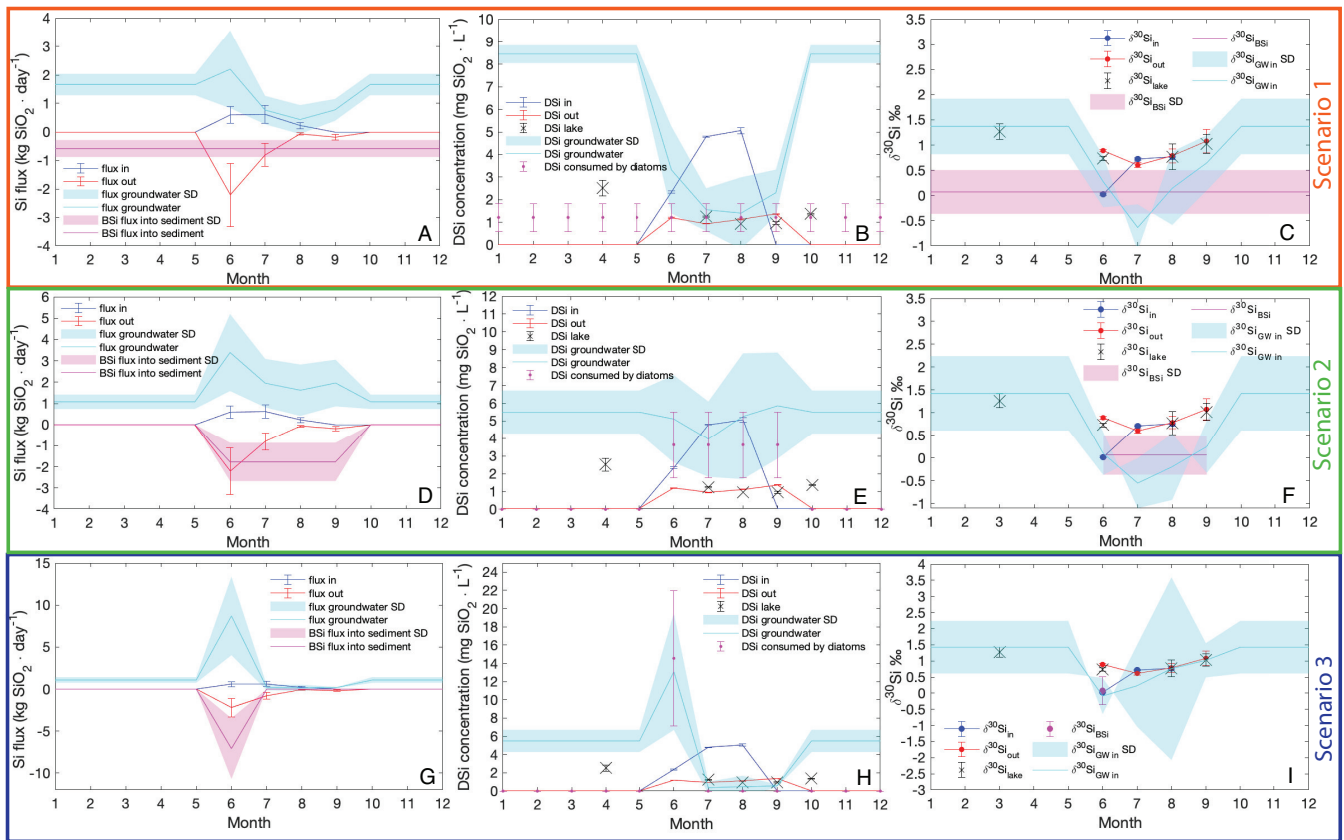
Figure B1. Inlet (blue), outlet (red), groundwater (cyan), and the BSi (magenta) fluxes, concentrations and isotopic composition. Scenario 1: A-C The constant BSi flux into sediment (A) influences the groundwater DSi concentration (B) and the silicon isotopic composition (C). Scenario 2: D-F present the effect of BSi flux adjusted to the diatom bloom season of 4 months (D) on the groundwater concentration (E) and isotopic composition (F). Scenario 3: G-I The diatom bloom represented by the BSi flux into the sediment is restricted to 1 month only. During June all BSi accumulated for 1 year is produced, and the groundwater concentration (H) and the isotopic composition (I) are affected.

concentration $(8.46 \pm 0.40\,\mathrm{mg\,SiO_2\,l^{-1}})$, groundwater discharge, lake volume change during the ice-covered period, and the difference of the isotopic composition of the lake water between September $(1.02 \pm 0.24‰)$ and March $(1.27 \pm 0.10‰)$, the isotopic ratio of the groundwater is calculated to be $1.37 \pm 0.55‰$ (Figure B1C).

B2 Scenario 3: only 1 month of BSi flux into the sediment

The third scenario is based on the inlet and outlet DSi fluxes but assumes that diatom production occurs only in June. This scenario could occur if the climate would experience cooling and the diatom growth period would be extremely shortened. Additionally, this scenario demonstrated the highest groundwater concentrations during the diatom growing season. The rest of the year diatom production, and so the BSi flux into the sediment, is negligible or zero. Therefore, the yearly accumulated BSi

settles into the sediment within one month, which yields a BSi flux of 7.08 ± 3.62 kg SiO_2 per day (magenta line, Figure B1G). In this scenario, groundwater input must be from 0.15 ± 0.37 kg SiO_2 to 8.70 ± 4.59 kg SiO_2 per day, and the DSi concentration ranges between 0.38 ± 0.66 mg SiO_2 l^{-1} to 13.10 ± 6.41 mg SiO_2 l^{-1} during the ice-free period (cyan line, Figure B1H). Similar to the second scenario (in the main text), to restore the lake DSi concentration during the ice-covered period from lake-October to mid-June, groundwater DSi concentration is around 5.50 ± 1.22 mg SiO_2 l^{-1}.

Scenario 3 assumes the BSi flux into the sediment occurs only in June, and the rest of the year there are no processes causing stable Si isotope fractionation. This scenario originates from data in August and September, when the δ^{30}Si of inlet, outlet and the lake are very similar. Only in June is there fractionation between the lake stream inlets and the lake, which is described by the open-system-fractionation model. Therefore, the groundwater concentration in June increases to 13.10 ± 6.41 mg SiO_2 l^{-1} (Figure B1H), with an isotopic ratio of -0.09 ± 0.56‰ (Figure B1I) to sustain the diatom production represented by BSi flux into the sediment. The production consumes 88% of the available DSi.

In July, August, and September the groundwater DSi concentration is low, as the lake does not have any production, thus no demand on the DSi. The isotopic composition of the groundwater is 0.38 ± 0.66‰, 0.48 ± 1.19‰, and 0.57 ± 0.14‰, respectively (Figure B1I). High uncertainties in the isotopic composition of the groundwater reflect the uncertainties in the stream and groundwater discharges and fluxes.

Appendix C: Discussion: Scenarios evaluation

Scenarios 1 and 3 of Si mass balance (Table B1, Figure B1A and G) are demonstrating how the groundwater concentration would change with changes of length of diatom production. It is likely that the diatom growth season would be driven by the changes in climate and thus the ice-free period length. Our models aimed to estimate the changes in the lake DSi and Si balance in those extreme changes of growing season driven by changes in climate. However, the groundwater concentrations are commonly higher than the superficial streams (Frings et al., 2016; Maavara et al., 2018; Opfergelt et al., 2011), which is not the case in scenario 1 and 3. The groundwater DSi concentrations are lower than in the stream inlet during the ice-free period in those two scenarios (Figure B1B and B1H), which suggest that those scenarios have either missing or surplus data of the inlet and outlet DSi concentration and discharges. A more complex model with variable discharges of groundwater and stream inlets and outlet depending on precipitation end evaporation changes would be needed. Therefore, those two scenarios bring only a rough estimate hinting the changes in DSi and Si isotopic mass balances connected to changes in climate.

Supplementary material

Table S1. Summary of all samplings of Lake 850

Site Description	Coordinates	Max Depth	Sampling Depth	Sampling Date	Sample Type	Sample number
Inlet 1	N 68°17′50.6″ E19°7′6.9″	5 cm		26/Jun/18	water, Q	n=2
				03/Jun/19		
Inlet 2	N 68°17′53.5″ E19°7′8.3″	6 cm		13/Jul/19	water, Q	n=3
				22/Aug/19		
				20/Sept/19		
Outlet	N 68°17′54.8″ E19°7′26.3″	10 cm		26/Jun/18	water, Q	n=5
				03/Jun/19		
				13/Jul/19		
				22/Aug/19		
				20/Sept/19		
Lake water	N 68°17′51.3″ E19°7′10.3″		surface	03/Jun/19	water	n=1
Water profile	N 68°17′53.5″ E19°7′15.6″	4.2-7.5 m	1 m to 7 m	22/Mar/19	water	n=14
				22/Aug/19		
				20/Sept/19		
Rn sampling 100	N 68°17′53.1″ E19°7′20.4″	0.75 m	0.5 m	22/Aug/19	water	n=1
Rn sampling 101	N 68°17′53.5″ E19°7′16.9″	7.5 m	1.5-4 m	22/Aug/19	water	n=2
Rn sampling 102	N 68°17′54.2″ E19°7′18.7″	4 m	1.5 m	22/Aug/19	water	n=1
Rn sampling 103	N 68°17′51.5″ E19°7′11.7″	2 m	1.5 m	22/Aug/19	water	n=1
Rn sampling 104	N 68°17′53.3″ E19°7′11.9″	5 m	1.5 m	22/Aug/19	water	n=1
Rn sampling 20	N 68°17′54.4″ E19°7′21.4″	0.9 m	0.5 m	20/Sept/19	water	n=1
Rn sampling 21	N 68°17′54.8″ E19°7′18.2″	5.4 m	1.5 m	20/Sept/19	water	n=1
Rn sampling 22	N 68°17′52.7″ E19°7′12.0″	4.2 m	1.5 m	20/Sept/19	water	n=1
Rn sampling 23	N 68°17′53.2″ E19°7′17.7″	6.1 m	1.5-4 m	20/Sept/19	water	n=2
Rn sampling 24	N 68°17′52.5″ E19°7′16.6″	4.2 m	1.5 m	20/Sept/19	water	n=1
HTH gravity core 1	N 68°17′53.2″ E19°7′17.2″	7.6 m	15 cm	22/Mar/19	sediment	n=1
HTH gravity core 2	N 68°17′52.9″ E19°7′14.1″	6.8 m	33 cm	22/Aug/19	sediment	n=1
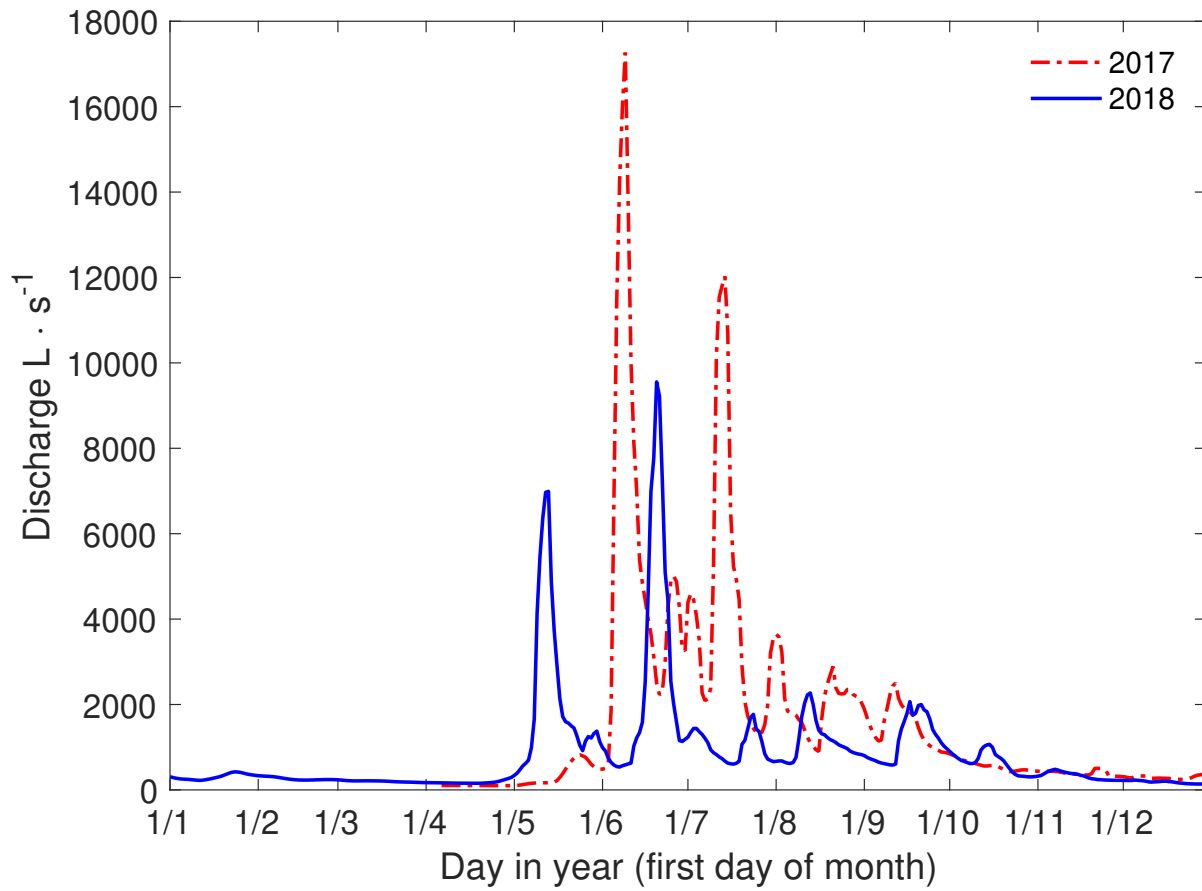
Figure S1. Daily mean discharge in $1s^{-1}$ of neighbouring river Miellejohka in years 2017 and 2018 (ANS, 2020b)
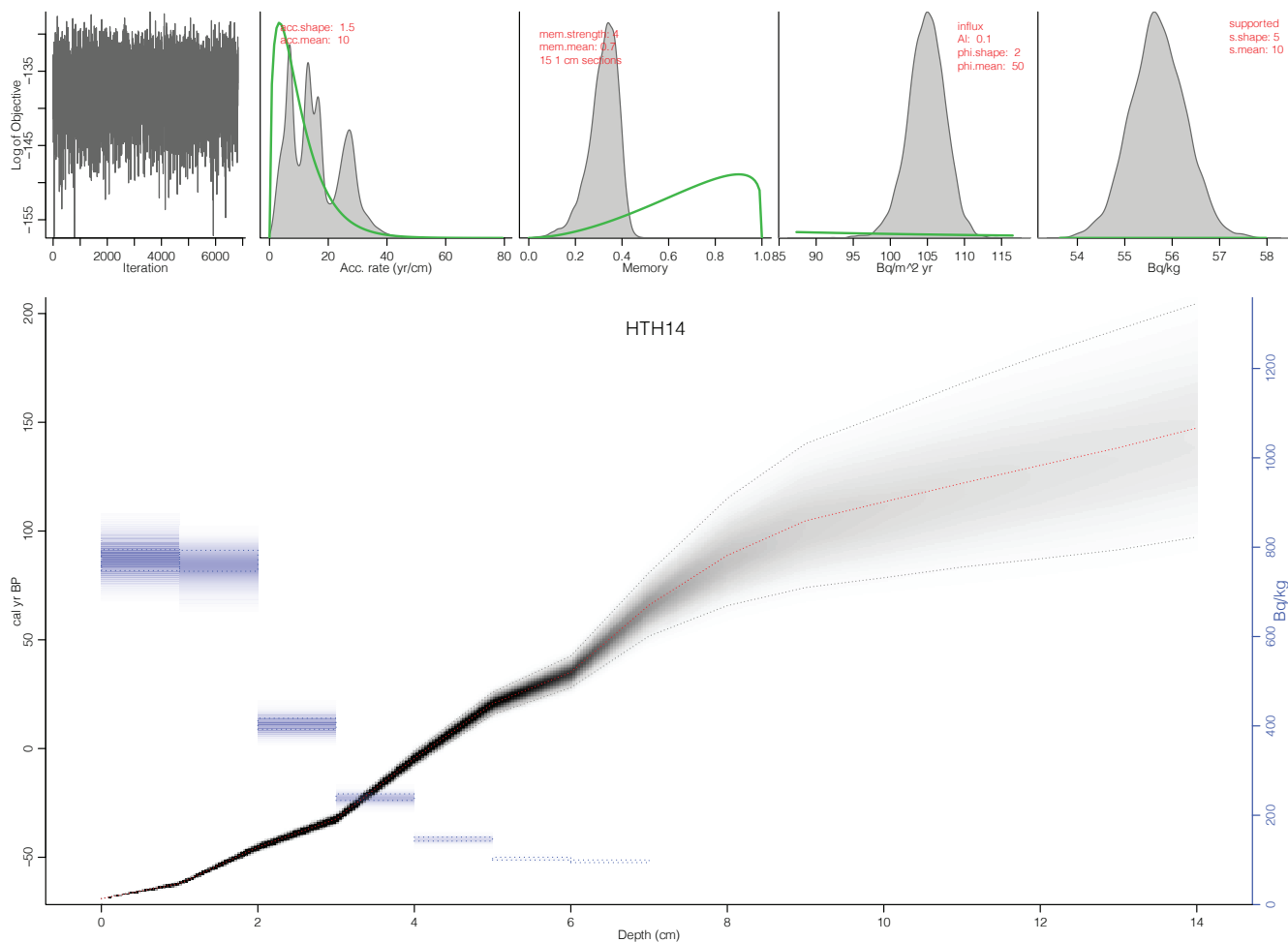
Figure S2. Age-depth model of the gravity core. Red line is the median probability age from all age-depth iterations. Grey shading represents age model probability and contains 95% confidence interval (dashed lines). The blue rectangles are the unsupported ^{210}Pb concentration in $\mathrm{Bq\,kg^{-1}}$. Iteration history (left inset), prior and posterior densities of the mean accumulation rate (second left inset), and prior and posterior of the memory (middle inset), the ^{210}Pb influx (second right inset), and supported ^{210}Pb in $\mathrm{Bq\,kg^{-1}}$ (right inset).